AD 405 131

NWL Report No. 1853

ROTATING FLOWS NORMAL TO A FLAT SURFACE

by

Ernst W. Schwiderski and Hans J. Lugt
Computation and Analysis Laboratory

U. S. NAVAL WEAPONS LABORATORY
DAHLGREN, VIRGINIA

U. S. Naval Weapons Laboratory
Dahlgren, Virginia

Rotating Flows Normal

To a Flat Surface

by

Ernst W. Schwiderski and Hans J. Lugt
Computation and Analysis Laboratory

NWL REPORT NO. 1853

Task Assignment
NO. R360FR103/2101/R01101001

April 1963

TABLE OF CONTENTS

ABSTRACT

Numerical solutions of three-parameter vortex flows over flat surfaces and of rotating flows of von Kármán's and Bödewadt's types are presented for a variety of Reynolds numbers. The results have been obtained on the basis of an extended boundary layer theory, which allows a reduction of the Navier-Stokes equations to a set of Volterra integral equations. The new flows are in good agreement with available physical observations.

FOREWORD

This work was sponsored by the Naval Weapons Laboratory Foundational Research Program. It was performed in the Computation and Analysis Laboratory as part of the Meteorological and Oceanographical project (R360FR103/2101/R01101001).

The authors wish to extend their thanks to Dr. C. J. Cohen for many critical and stimulating discussions.

The date of completion was 10 April 1963.

Approved for Release:

/s/ R. H. LYDDANE
Technical Director

1. Introduction

Rotating flows normal to a flat surface have been studied in [10] and [11] on the basis of an extension of Prandtl's boundary layer theory. The investigations in [10] dealt with the vortex motion of a viscous fluid, which is produced by a very long rod normal to a flat surface (see Figure 1). In [11] the rotating flows of von Kármán and Bödewadt, which are generated by a rotating flat plate in a fluid at rest or by a fluid in solid-body rotation over a fixed plate, are re-examined. In all three cases the Navier-Stokes equations have been reduced to sets of nonlinear ordinary differential equations, which are connected with appropriate boundary data.

In the present paper the nonlinear boundary value problems are transformed into equivalent sets of nonlinear Volterra integral equations, which can be solved by efficient iteration procedures. Complete numerical results for all three problems have been computed and are displayed in the following sections for a selected variety of Reynolds numbers. Characteristic properties of these flows are pointed out and compared with actually observed phenomena. In particular, the properties of vortex flows over flat surfaces are compared with phenomena observed in hurricanes. Although the vortex models considered are only very rough approximations to real hurricanes, the qualitative agreement is satisfactory.

It is a distinctive feature of all flows considered, that they depend on three characteristic parameters. This is a result of the complete boundary data which have been deduced from physical flow models in order to specify a unique solution of the elliptic Navier-Stokes equations. Because of the great importance of this procedure for the theory of real flows, it seems worthwhile to insert here a simple example, which displays the fundamental dependence properties of the solutions of the Navier-Stokes equations.

As is shown, for instance, in [9] the Couette flows between a fixed plate and a moving parallel plate depend on the kinematic viscosity of the fluid, the speed of the moving plate, the distance of the parallel plate, and the constant pressure gradient. In addition to these four characteristic parameters the Couette flows are also specified by the well-known similarity assumption. While the similarity assumption restricts the type of the singularities which are permitted at the entrance and the exit of the flow field, the constant pressure gradient specifies their strengths. If the moving plate is removed, one obtains similar flows along an infinite plate which depend on three characteristic parameters.

It is one of the most significant features of the extended boundary layer theory and the integration procedure developed in [10] that the correct dependence properties of real flows are preserved. The classical boundary layer theory loses this property by truncating the elliptic Navier-Stokes equations to parabolic

differential equations. This may be demonstrated by a simple example, which shows the basically different dependence properties of solutions of elliptic and parabolic partial differential equations.

The elliptic Laplace equation

$$u_{xx} + u_{yy} = 0 \qquad (*)$$

yields regular solutions in the unit square $[0 \le x \le 1,\ 0 \le y \le 1]$ for any boundary data, which are, e.g., piecewise continuous. However, the parabolic differential equation

$$u_{yy} = 0 \qquad (**)$$

with the general solution

$$u = f(x)y + g(x)$$

does not allow the prescription of boundary values along $x = 0$ and $x = 1$ in addition to data at $y = 0$ and $y = 1$. For instance, if the boundary data $u(x,0) = u(x,1) = 0$, $u(0,y) = \epsilon_1(y)$, and $u(1,y) = \epsilon_2(y)$ are imposed, no solution exists to the parabolic equation (**) no matter how small $|\epsilon_1(y)| \not\equiv 0$ and $|\epsilon_2(y)| \not\equiv 0$ may be assumed.

In the problems of von Kármán and Bödewadt uniqueness has been achieved by very restrictive similarity assumptions, which indirectly determine the well-known sink and source distributions of infinite initial velocities at large distances from the axes of rotation. Consequently, the physical models of these flows remain unknown.

This has first been pointed out by Stewartson (see [4, 5, 13]) who questioned the physical meaning of the oscillating Bödewadt flow. Moore (see [4, 5]) doubted also the usefulness of the Bödewadt solution, because the flow shows no tendency of boundary layer separation from the surface at the axis of rotation. This should be expected as the secondary flow is of wake type (see [12]). Indeed, simple experiments in a tea cup (see [4]) display very clearly a separation of the fluid from the bottom of the cup. When the stirring of the tea is sufficiently slow, tea leaves move toward the axis of rotation and heap up at the bottom of the cup. However, when the stirring is sufficiently fast, the tea leaves settle distinctly on a ring around the axis of rotation. This interesting phenomenon is a graphic demonstration of a separated wake flow along the axis of rotation. It is comparable with the settling of dust around corners of rooms which are not well kept. While the dust settles on rings around the corners, the corners themselves remain clean. This also indicates a separated wake in the corner into which no dust particles can enter.

Another peculiar result, which concerns both the von Kármán and the Bödewadt flows, is the constant "deviation angle" of the spiral motion from a circular motion at the surface of the plate (see [9]). Since the secondary radial velocity depends strongly on the primary tangential velocity (compare [10]), it should be expected that the

deviation angle of the streamlines at the plate would depend on a Reynolds number. The flows of von Kármán and Bödewadt do not fulfill this expectation, which seems to indicate that these flows are considerably affected by the strong sinks and sources assumed at large distances from the axes of rotation.

2. Vortex Flows Normal to a Plate

An axisymmetric vortex flow over a flat surface has been defined in [10] as a solution of the Navier-Stokes equations

$$uu_r + wu_z - \frac{v^2}{r} = -\frac{1}{\rho} p_r + \nu\left[u_{rr} + \left(\frac{u}{r}\right)_r + u_{zz}\right] \tag{1}$$

$$uv_r + wv_z + \frac{uv}{r} = + \nu\left[v_{rr} + \left(\frac{v}{r}\right)_r + v_{zz}\right] \tag{2}$$

$$uw_r + ww_z = -\frac{1}{\rho} p_z + \nu\left[w_{rr} + \frac{1}{r} w_r + w_{zz}\right] \tag{3}$$

$$(ru)_r + (rw)_z = 0 \tag{4}$$

by the boundary data

$$\left.\begin{matrix} r > 0 \\ z = 0 \end{matrix}\right\} : \quad u = 0,\ v = 0,\ w = 0 \tag{5}$$

$$\left.\begin{matrix} r = \infty \\ z < \infty \end{matrix}\right\} : \quad u = 0,\ v = 0,\ w = 0 \tag{6}$$

$$\left.\begin{matrix} r \to 0 \\ z > 0 \end{matrix}\right\} : \quad u \to 0,\ \frac{rv}{\Gamma} \to 1,\ \frac{w}{\Gamma A \log \frac{r_0}{r}} \to 1 \tag{7}$$

$$\left.\begin{matrix} r < \infty \\ z \to \infty \end{matrix}\right\} : u \to 0,\ \frac{rv}{\Gamma} \to 1,\ \frac{w}{\Gamma A \log \frac{r_0}{r}} \to 1. \tag{8}$$

In these equations u, v, and w denote the velocity components of the vortex flow which correspond to the coaxial cylindrical coordinate system (r, φ, z). The variable pressure and the constant density and kinematic viscosity of the fluid are designated by p, ρ, and ν. While the vortex strength Γ and the radial extension r_o of the axial logarithmic sink (see Fig. 1) are at one's disposal, the constant value of A must be determined simultaneously with the solution.

Guided by an extension of Prandtl's boundary layer theory a first order reduction of the Navier-Stokes equations to an ordinary boundary value problem has been found in [10], which is valid in the vicinity of the line $r = r_o$. This approximation was achieved with the aid of the limiting line $z = \delta(r)$ of the boundary layer along the surface at $z = 0$. This limiting line was defined by the ϵ - condition

$$v(r,z) = \frac{\Gamma}{r}(1 - \epsilon) \tag{9}$$

and remained to be found together with the primary tangential velocity v.

After applying the following similarity transformation

$$r = r, \ \zeta = \frac{z}{\delta(r)}, \ R = \frac{\Gamma}{\nu} \ (= \text{Reynolds number}) \tag{10}$$

$$u = \frac{\Gamma}{r} U(\zeta), \ v = \frac{\Gamma}{r} V(\zeta), \ w = \Gamma A \log \frac{r_o}{r} W(\zeta), \ \frac{p}{\rho} = -\frac{\Gamma^2}{2r^2} P(\zeta) \tag{11}$$

$$U = -\dot{G}(\zeta), \ W = \frac{1}{G_\infty}\left[G(\zeta) - \zeta\dot{G}(\zeta)\right] \tag{12}$$

one arrives at the following ordinary differential equations

$$\dddot{G} + \sigma^3 \zeta \ddot{G} = \frac{R\sigma^3}{4} (\dot{G}^2 + V^2 - P) \tag{13}$$

$$\ddot{V} + \sigma^2 \zeta \dot{V} = 0 \tag{14}$$

$$\dot{G}(G - \zeta \dot{G}) = \frac{1}{2\sigma^2} \dot{P}, \tag{15}$$

which must be integrated under the boundary conditions

$$\zeta = 0: \quad G = 0, \dot{G} = 0, V = 0, \tag{16}$$

$$\zeta = \infty: \quad G = G_\infty , V = 1, P = 1. \tag{17}$$

Simultaneously with this reduction one obtains the equation of the limiting line of the boundary layer in the vicinity of $r = r_0$ in the form (see Fig. 1)

$$z = \delta(r) = \sigma \frac{r_0}{2} \left(\frac{r}{r_0}\right)^2 \left(1 + 2 \log \frac{r_0}{r}\right) . \tag{18}$$

The constant value A is

$$A = 2 \frac{\sigma}{r_0} G_\infty , \tag{19}$$

where the characteristic parameter σ is determined by the ϵ - condition

$$\zeta = 1: \quad V = 1 - \epsilon. \tag{20}$$

For an integration of the remaining ordinary boundary value problem it is convenient to introduce the following new variables

$$\eta = \sigma\zeta \quad \text{and} \quad g = \sigma G. \tag{21}$$

This substitution leads to the differential equations

$$\dddot{g} + \eta\ddot{g} = \frac{R}{4}\,(\dot{g}^2 + V^2 - P) \tag{22}$$

$$\dot{g}(g - \eta\dot{g}) = \frac{1}{2}\,\dot{P} \tag{23}$$

with

$$V(\eta) = \operatorname{erf}\frac{\eta}{\sqrt{2}} = \frac{2}{\sqrt{\pi}}\int_0^{\frac{\eta}{\sqrt{2}}} e^{-t^2}dt, \tag{24}$$

which must be integrated under the boundary conditions

$$\eta = 0: \quad g = 0, \ \dot{g} \neq 0, \tag{25}$$

$$\eta = \infty: \quad g = g_\infty, \ P = 1. \tag{26}$$

The ordinary boundary value prpblem defined by the equations (22) through (26) has been solved for the Reynolds number R = 10 by the Runge-Kutta method which started the integration with an assumed set of initial data that had to be improved successively until the boundary condition (26) was sufficiently met. The result of this integration

has been displayed in [10]. The inefficiency of this method is obvious because two initial conditions must be found which correspond to the two ignored boundary conditions (26).

For an efficient integration of the remaining ordinary boundary value problem it is convenient to transform the differential equations (22) and (23) with the boundary conditions (25) and (26) into an equivalent integral equation (see [14]). Assuming that the auxiliary function

$$D(\eta) = P(\eta) - \dot{g}^2(\eta) - V^2(\eta) \tag{27}$$

is known, then the differential equation (22) reduces to the linear equation

$$\ddot{g} + \eta\dot{g} = -\frac{R}{4} D(\eta) \tag{28}$$

which is integrable by quadrature. Indeed, with the aid of the error function (24) one finds the general solution of (28) in the form

$$\dot{g}(\eta) = \lambda V(\eta) + \bar{\lambda} - \frac{R}{4}\int_0^\eta \frac{D(t)}{\dot{V}(t)} \left[V(\eta) - V(t)\right] dt \,. \tag{29}$$

The boundary conditions (25) and (26) lead then to the nonlinear Volterra integral equation

$$\dot{g}(\eta) = \lambda V(\eta) - \frac{R}{4}\int_0^\eta \frac{D(t)}{\dot{V}(t)} \left[V(\eta) - V(t)\right] dt \tag{30}$$

for $\dot{g}(\eta)$, where

$$\lambda = \frac{R}{4}\int_0^\infty \frac{D(t)}{\dot{V}(t)}\left[1 - V(t)\right] dt. \tag{31}$$

The functions $g(\eta)$ and $P(\eta)$ are obtained by direct integration of the equations (30) and (23) under the boundary conditions (25) and (26). They are

$$g(\eta) = \int_0^\eta \dot{g}(t)dt \tag{32}$$

and

$$P(\eta) = \mu + g^2(\eta) - 2\int_0^\eta t\dot{g}^2(t)dt, \tag{33}$$

where

$$\mu = P(0) = 1 - g_\infty^2 + 2\int_0^\infty t\,\dot{g}^2(t)dt. \tag{34}$$

This concludes the transformation of the boundary value problem under consideration into a set of Volterra integral equations. It is, vice versa, not difficult to show that any solution of the integral equations is a solution of the boundary value problem. Thus the transformation applied is an identical transformation.

The integral equations (30), (32), and (33) have been numerically integrated for a variety of Reynolds numbers. Some selected solutions will be discussed in the following section. All solutions have been constructed by an iteration procedure (see [10]), which successively improved an appropriate first approximation. It was found that the method is very efficient, provided the first approximation is sufficiently close to the correct solution.

For small Reynolds numbers the iterations can be started with

$$g(\eta) \equiv 0, \quad P(\eta) \equiv 1 \tag{35}$$

as adequate first approximations. For larger Reynolds numbers the iterations may be started by solutions, which are obtained for smaller Reynolds numbers. In order to improve the rate of convergence of the iteration procedure, especially in cases where the iteration is started with a very crude approximation, it is helpful to average the outcoming solution with the entering approximation of the iteration by means of appropriate weighting factors.

3. Properties of Vortex Flows

Axisymmetric vortex flows normal to a flat surface have been computed and tabulated for various Reynolds numbers (see Tables 1, 2 and 3). Examples have been selected and plotted in the figures 3, 4, and 5.

The numerical results confirm the phenomena of vortex flows which were pointed out in [10]. It may be emphasized that the numerical calculations of all vortex flows computed indicated no symptoms of instability of the flow near the line $r = r_0$ (see Fig. 1 and compare [12]). Accordingly, vortex flows seem to remain laminar and attached to the surface for all Reynolds numbers at least in the vicinity of $r = r_0$. Nevertheless, since the secondary flow is of "wake type" (see [12]) within the cylinder $r = r_0$, separation of the flow should be expected to occur in the neighborhood of the vortex axis. However, outside the cylinder $r = r_0$ the secondary flow is of "stagnation type" and tends to prevent any flow separation. Thus, the instability in the motion, which is caused by a flow separation at the axis, seems to fade away when the flow changes its character. This explains the fact that the radial velocity U remains free of inflection points which characterize unstable flows.

As was explained in [10] vortex flows normal to a flat surface represent approximate models of hurricanes, provided exterior disturbances of the vortex flows other than those caused by the surface of the earth are excluded. Consequently, the numerical results may be compared with phenomena observed outside the cores of hurricanes. Despite the fact that real hurricanes are highly distorted by the tremendous rainfall inside the circle $r = r_0$, by the change of the density and the turbulence of the air, etc., the agreement with available observations appears to be satisfactory.

Indeed, the observations confirm the wake and stagnation character of the secondary flow, where the rainfall area coincides roughly with the circular region $r \leq r_0$. The rapidly increasing rainfall toward the core of a hurricane (see [15,p.130]) is indicated by the logarithmic increase of the axial velocity toward the vortex axis. The strong dependence of the secondary flow upon the Reynolds number R (see Fig. 3 , 4 , and 5) indicates a radial shear stress at the surface, which is large compared with the tangential shear stress. This explains the very strong radial ocean waves produced by hurricanes which are known as ocean swells (see [7 , p.298]). As can be deduced from figure 3 , inside the cylinder $r = r_0$ the secondary flow near the surface converges to the surface before it finally leaves the vicinity of the surface in the normal direction (see Fig. 1). According to Riehl this remarkable phenomenon has also been observed in hurricanes (see [7 , p. 320]).

In order to get a rough idea of the boundary layer thickness near the core of a hurricane, one may consider a hurricane of average size, which has a rainfall area of about $2r_0 \approx 2000$ km in diameter (see [15,p.130]). If the limiting line of the boundary layer $z = \delta(r)$ (see Eq. (18)) is determined to a relative accuracy of $\epsilon_r = 1\%$, then the characteristic parameter σ was found to be $\sigma \approx 2.5$ (see [10]). With these assumptions the boundary layer thickness at the edge of the hurricane core,which is at $r \approx 30$ km from the vortex axis (see [7 p.297]), can be computed by equation(18), which yields $\delta \approx 9$ km.

This result explains the observed thick boundary layers (see [6]), which are produced by the friction forces along the surface of the earth in hurricanes.

4. Von Kármán and Bödewadt Flows

The rotating flows of von Kármán ($\gamma = 0$) and Bödewadt ($\gamma = 1$) have been defined in [11] as solutions of the Navier-Stokes equations (1) through (4) by the boundary data (see Fig. 2).

$$\left.\begin{matrix} |r| < \infty \\ z = 0 \end{matrix}\right\} : \quad u = 0,\ v = (1 - \gamma)\omega r,\ w = 0 \tag{36}$$

$$\left.\begin{matrix} |r| \leq \infty \\ z = \infty \end{matrix}\right\} : \quad u = 0,\ v = \gamma\,\omega\, r,\ w = w_\infty \tag{37}$$

$$\left.\begin{matrix} |r| \to \infty \\ z > 0 \end{matrix}\right\} : \frac{u}{\omega r} \to 0,\ \frac{v}{\omega r} \to \gamma,\ w \to w_\infty\ . \tag{38}$$

In both problems the angular velocity ω and the constant w_∞, which determines the strengths of the singularities at the points ($r = \pm \infty$, $z = 0$), are at one's disposal.

After introducing the limiting line of the boundary layer in the form

$$z = \delta(r) = a - br^2 + \ldots\ , \tag{39}$$

which is determined by the ϵ-condition

$$z = \delta(r):\ \frac{v(r,z)}{\omega r} = \gamma + (-1)^\gamma\,\epsilon, \tag{40}$$

the Navier-Stokes equations can be reduced around r = 0 to a set of ordinary differential equations. This first order reduction requires the following similarity transformation

$$r = r,\ \zeta = \frac{z}{\delta(r)}\ ,\ \ \frac{p}{\rho} = \frac{\omega^2 r^2}{2}\,\gamma - \frac{w_\infty^2}{2}\,P(\zeta) \tag{41}$$

$$u = \omega\, r\, U(\zeta),\ \ v = \omega\, r\, V(\zeta),\ \ w = w_\infty\, W(\zeta) \tag{42}$$

$$U = -\,\dot{G}(\zeta),\ W = \frac{G(\zeta)}{G_\infty}\ ,\ P = \frac{H(\zeta)}{G_\infty^2} \tag{43}$$

and the following conventions about the constants

$$R = \frac{\omega}{\nu}\,\frac{a}{b}\ ,\ \sigma^2 = ab,\ w_\infty = 2\omega\, aG_\infty. \tag{44}$$

The similarity transformation leads to the ordinary differential equations (see [11])

$$\dddot{G} + 2\sigma^2(4\zeta - RG)\ddot{G} + \sigma^2 R(\dot{G}^2 - V^2 + \gamma - 4\sigma^2\zeta\dot{H}) = 0 \tag{45}$$

$$\ddot{V} + 2\sigma^2(4\zeta - RG)\dot{V} + 2\sigma^2 R\dot{G}V = 0 \tag{46}$$

$$\ddot{G} + 2\sigma^2(2\zeta - RG)\dot{G} + \sigma^2 R\dot{H} = 0, \tag{47}$$

which must be integrated under the boundary conditions

$$\zeta = 0:\ \ G = 0,\ \dot{G} = 0,\ V = 1 - \gamma \tag{48}$$

$$\zeta = \infty:\ \ G = G_\infty,\ V = \gamma,\ H = G_\infty^2. \tag{49}$$

When the solution is found for a specified Reynolds number R, the ϵ-condition

$$\zeta = 1:\ \ V = \gamma + (-1)^\gamma\,\epsilon \tag{50}$$

determines the characteristic parameter σ. Thus, the unknown coefficients a and b of the parabolic limiting line of the boundary layer (39) and the corresponding w_∞ can be computed from equations (44). As was shown in [11], in physical applications the ratio a/b may roughly be computed by

$$\frac{a}{b} = \left(\frac{\beta}{2}\right)^2 \tag{51}$$

where β represents the diameter of an appropriate finite flow model (see Fig. 2).

The corresponding finite flow models, which were described in [11] and which are sketched in figure 2, show graphically the dependence of the von Kármán and Bödewadt flows on 3-parameter Reynolds numbers. Indeed, if the slit between the cylinder and the disk is of negligible size, the finite flow model depends on four essential parameters: the kinematic viscosity ν of the fluid, the angular velocity ω of the rotating disk or the rotating cylinder, and the height α and the diameter β of the cylinder containing the fluid. When carrying out the limits $\alpha \to \infty$ and $\beta \to \infty$, one parameter, for instance, the ratio α/β emerges as a characteristic parameter for the infinite flow model. In accordance with the Reynolds number (44) it is useful to replace the ratio α/β by the ratio a/b as a parameter at one's disposal. Hence, a finite flow model may be considered similar to an infinite model if they both agree in the ratios a/b, that is, in the products

of the boundary layer thickness a and the radius of curvature 1/2b at the axes of rotation (see equation (39)).

As in the vortex problem (Section 2) it is helpful to transform the remaining boundary value problem into equivalent Volterra integral equations. This transformation may be carried out after introducing the following new scales for all variables concerned:

$$\eta = \sigma\zeta, \quad g = \sigma G, \quad h = \sigma^2 H \quad . \tag{52}$$

In the new variables the equations (45), (46), and (47) assume the following form

$$\ddot{g} + 8\eta\dot{g} = -RA(\eta), \quad A(\eta) = \gamma + \dot{g}^2 - 2g\ddot{g} - V^2 - 4\eta\dot{h} \tag{53}$$

$$\ddot{V} + 8\eta\dot{V} = -RB(\eta), \quad B(\eta) = 2(\dot{g}V - g\dot{V}) \tag{54}$$

$$\dot{h} = 2g\dot{g} - \frac{1}{R}(\ddot{g} + 4\eta\,\dot{g}) \quad . \tag{55}$$

These equations must be integrated under the boundary conditions

$$\eta = 0: \quad g = 0, \quad \dot{g} = 0, \; V = 1 - \gamma \tag{56}$$

$$\eta = \infty: \quad g = g_\infty = \text{finite}, \; V = \gamma, \; h = g_\infty^2 \tag{57}$$

With the aid of the error function

$$E(\eta) = \operatorname{erf}(2\eta) = \frac{2}{\sqrt{\pi}}\int_0^{2\eta} e^{-t^2}dt \quad , \tag{58}$$

the solutions of the boundary value problem obtained are exactly the solutions of the following set of Volterra integral equations:

$$\dot{g}(\eta) = \lambda_1 E(\eta) - R\int_0^{\eta} \frac{A(t)}{\dot{E}(t)} [E(\eta) - E(t)]\, dt \tag{59}$$

$$V(\eta) = 1 - \gamma + \lambda_2 E(\eta) - R\int_0^{\eta} \frac{B(t)}{\dot{E}(t)} [E(\eta) - E(t)]dt \tag{60}$$

$$h(\eta) = \lambda_3 + g^2 - \frac{\dot{g}}{R} - \frac{4}{R}\int_0^{\eta} t\dot{g}(t)dt \tag{61}$$

with

$$\lambda_1 = R\int_0^{\infty} \frac{A(c)}{\dot{E}(t)} [1 - E(t)]dt \tag{62}$$

$$\lambda_2 = 2\gamma - 1 + R\int_0^{\infty} \frac{B(t)}{\dot{E}(t)} [1 - E(t)]dt \tag{63}$$

$$\lambda_3 = \frac{4}{R}\int_0^{\infty} t\dot{g}(t)dt \quad . \tag{64}$$

The solutions of the integral equations (59) through (61) may be obtained by an iteration procedure which successively improves suitable first approximations. Numerical calculations have shown that for small Reynolds numbers R the iterations can be started with

$$g \equiv 0,\ h \equiv 0,\ V = 1 - \gamma + (2\gamma - 1)E(\eta). \tag{65}$$

For larger Reynolds numbers R the iterations may be initiated by solutions, which are obtained for smaller Reynolds numbers.

5. Properties of von Kármán and Bödewadt Flows

Rotating flows of von Kármán and Bödewadt have been computed and are presented in the tables 4 through 11 and in the figures 6 through 12.

The numerical calculations of von Kármán's flows indicated no tendency of flow separation near the axis of rotation for any Reynolds number. Since the secondary flow is of stagnation type (see [12])all velocity profiles are free of inflection points which characterize unstable flows (see [9, 12]). Accordingly, the boundary layers of von Kármán's type are considerably decreasing in thickness as the Reynolds number increases (see Fig. 7).

In contrast to the von Kármán flows the fluid motions of Bödewadt's type remain stable only below a certain critical Reynolds number, which has been computed to be

$$R_c \approx 8. \tag{67}$$

For Reynolds numbers $R \leq 8$ the Bödewadt flows are not oscillating and indicate no tendency of boundary layer separation at the axis of rotation. For Reynolds numbers $R \geq 9$ no proper nonoscillating flows exist, which indicates the existence of a separated flow around the axis of symmetry (compare [12]). It may be mentioned that this phenomenon has been carefully checked by changing the input data which determine the accuracy of the numerical method applied. In addition, the results have been rechecked by the Runge-Kutta method which has been applied to solve the equivalent system of differential equations. The high accuracy of both numerical methods and the stability of the solutions may be displayed by presenting the corresponding results of both methods in table form (see Tables 12 and 13) for the Reynolds number $R = 1$. In this connection it may be mentioned that the

Runge-Kutta method used only five digit initial values, which were obtained by the integral equation method. It can be seen that even the higher order derivatives of the velocity profiles show no symptoms of inflection points or even oscillations. The same has been found for the Reynolds numbers 5 through 8. However, for the Reynolds number R = 9 the remarkable stability of Bödewadt's flows is clearly discontinued. As explained in [12] this result was anticipated, because the Bödewadt flows are of wake type, for which boundary layer separation should be expected. It is, indeed, a justification of the doubts which were raised by Stewartson and Moore against the solution of Bödewadt (see Section 1). Furthermore, this significant phenomenon can easily be confirmed by the tea-cup experiment described in Section 1.

Due to the wake character of the Bödewadt flows, the boundary layer thickness is roughly constant with respect to increasing Reynolds numbers (see Fig. 11). As was shown in [10], this property is also shared by the vortex motions over flat surfaces (see Fig. 4). Furthermore, almost invariant dimensionless tangential velocities V can be observed in both the solid-body rotation and the vortex motion along flat surfaces.

Special attention may be given to the secondary radial velocities of the flows of von Kármán (Fig. 6) and Bödewadt (Fig. 10) and the vortex flows over flat surfaces (Fig. 3). In all three cases agreement can be seen in the property that the dimensionless radial velocities U are very rapidly increasing with growing Reynolds numbers. Thus, while the tangential shear stress at the surface increases relatively

The numerical calculations of von Kármán's flows indicated no tendency of flow separation near the axis of rotation for any Reynolds number. Since the secondary flow is of stagnation type (see [12]) all velocity profiles are free of inflection points which characterize unstable flows (see [9, 12]). Accordingly, the boundary layers of von Kármán's type are considerably decreasing in thickness as the Reynolds number increases (see Fig. 7).

In contrast to the von Kármán flows the fluid motions of Bödewadt's type remain stable only below a certain critical Reynolds number, which has been computed to be

$$R_c \approx 8. \tag{67}$$

For Reynolds numbers $R \leq 8$ the Bödewadt flows are not oscillating and indicate no tendency of boundary layer separation at the axis of rotation. For Reynolds numbers $R \geq 9$ no proper nonoscillating flows exist, which indicates the existence of a separated flow around the axis of symmetry (compare [12]). It may be mentioned that this phenomenon has been carefully checked by changing the input data which determine the accuracy of the numerical method applied. In addition, the results have been rechecked by the Runge-Kutta method which has been applied to solve the equivalent system of differential equations. The high accuracy of both numerical methods and the stability of the solutions may be displayed by presenting the corresponding results of both methods in table form (see Tables 12 and 13) for the Reynolds number $R = 1$. In this connection it may be mentioned that the

slowly, the radial shear stress grows relatively fast. Figure 13 shows the "angle of deviation χ" between the spiral motions and an undisturbed circular motion at the surface, which is defined by

$$\tan \chi = - \lim_{z \to o} \frac{u(r,z)}{v(r,z)} = - \frac{U'(0)}{V'(0)} \quad . \tag{68}$$

In all three cases the absolute value of χ starts at zero as the Reynolds number increases from zero, which is in contradiction with von Kármán's and Bödewadt's solutions. However, the new results are physically plausible.

Finally, an interesting pressure distribution across the flow field can be seen in both the von Kármán (Fig. 9) and the Bödewadt flows (Fig. 12). In a pure stagnation flow without rotation (see [12]) the pressure is monotonically increasing toward a pressure high at the surface. The same is true for von Kármán's flows, except that near the surface the pressure is rapidly decreasing in order to attain a pressure low at the surface. Similarly, in pure wake flows (see [12]) the pressure is monotonically falling toward a low at the surface. Bödewadt's flows follow the same pattern up to a point near the surface, from which point on the pressure is rapidly rising toward a high at the surface. These phenomena appear also in von Kármán's solution (see [9]) and in vortex flows over flat surfaces (see Fig. 5).

REFERENCES

[1] Batchelor, G. H., Note on a class of solutions of the Navier-Stokes equations representing steady rotationally symmetric flow, Quarterly Journal of Mechanics and Applied Mathematics, 4, (1951), 29-41.

[2] Bödewadt, U. T., Die Drehströmung über festem Grunde, ZAMM, 20, (1940), 241 - 253.

[3] Von Kármán, Über laminare und turbulente Reibung, ZAMM, 1, (1921) 244 - 247.

[4] Mack, L. M., The laminar boundary layer on a disk of finite radius in a rotating flow, Jet Propulsion Laboratory, Technical Report No. 32 - 224, May 20, 1962.

[5] Moore, F. K., Three-dimensional boundary layer theory, Advances in Applied Mechanics, IV, (1956), 159 - 228.

[6] Palmén, E. and Riehl, H., Budget of Angular Momentum and Energy in Tropical Cyclones, Journal of Meteorology 14, 1957.

[7] Riehl, H., Tropical Meteorology, McGraw-Hill Book Co., Inc., 1954.

[8] Rogers, M. H. and Lance, G. N., The rotationally symmetric flow of a viscous fluid in the presence of an infinite rotating disk, Journal of Fluid Mechanics, 7, (1960), 617 - 631.

[9] Schlichting, H., Boundary Layer Theory, Fourth Edition, 1960.

[10] Schwiderski, E. W. and Lugt, H. J., Boundary Layer Along a Flat Surface Normal to a Vortex Flow, U. S. Naval Weapons Laboratory Report No. 1835, 1962.

[11] Schwiderski, E. W. and Lugt, H. J., Rotating Flows of Kármán-Bödewadt and Stagnation Flows, U. S. Naval Weapons Laboratory Report No. 1836, 1962.

[12] Schwiderski, E. W. and Lugt, H. J., Stagnation and Wake Flows Normal to a Flat Surface, U. S. Naval Weapons Laboratory Report No. 1840, 1963.

[13] Stewartson, K., On the Flow between Two Rotating Coaxial Disks, Proc. Cambridge Phil. Soc.,49,(1953), 333 - 341.

slowly, the radial shear stress grows relatively fast. Figure 13 shows the "angle of deviation χ" between the spiral motions and an undisturbed circular motion at the surface, which is defined by

$$\tan \chi = - \lim_{z \to o} \frac{u(r,z)}{v(r,z)} = - \frac{U'(0)}{V'(0)} \quad . \tag{68}$$

In all three cases the absolute value of χ starts at zero as the Reynolds number increases from zero, which is in contradiction with von Kármán's and Bödewadt's solutions. However, the new results are physically plausible.

Finally, an interesting pressure distribution across the flow field can be seen in both the von Kármán (Fig. 9) and the Bödewadt flows (Fig. 12). In a pure stagnation flow without rotation (see [12]) the pressure is monotonically increasing toward a pressure high at the surface. The same is true for von Kármán's flows, except that near the surface the pressure is rapidly decreasing in order to attain a pressure low at the surface. Similarly, in pure wake flows (see [12]) the pressure is monotonically falling toward a low at the surface. Bödewadt's flows follow the same pattern up to a point near the surface, from which point on the pressure is rapidly rising toward a high at the surface. These phenomena appear also in von Kármán's solution (see [9]) and in vortex flows over flat surfaces (see Fig. 5).

REFERENCES (Continued)

[14] Tricomi, F. G., Integral Equations, Interscience Publishers, Inc., New York, 1957.

[15] Handbuch der Physik, Bd. XLVIII, Geophysik II, Springer Verlag, 1957.

APPENDIX A

TABLE 1

RADIAL VELOCITY - U OF VORTEX FLOWS

η \ R	1	10	20	50	100	500
0	.0000	.0000	.0000	.0000	.0000	.0000
.1	.0172	.1273	.1985	.2880	.3779	.6384
.2	.0317	.2302	.3474	.4802	.5910	.7783
.3	.0436	.3093	.4513	.5963	.6935	.7791
.4	.0528	.3663	.5082	.6568	.7293	.7565
.5	.0594	.4034	.5468	.6779	.7263	.7277
.6	.0636	.4232	.5590	.6719	.7008	.6919
.7	.0657	.4283	.5546	.6474	.6622	.6489
.8	.0659	.4215	.5346	.6106	.6160	.6009
.9	.0645	.4052	.5034	.5660	.5656	.5499
1.0	.0618	.3818	.4648	.5170	.5133	.4981
1.1	.0581	.3534	.4291	.4660	.4610	.4467
1.2	.0537	.3220	.3843	.4149	.4097	.3969
1.3	.0488	.2890	.3466	.3652	.3604	.3495
1.4	.0437	.2559	.3025	.3180	.3140	.3049
1.5	.0386	.2236	.2604	.2739	.2708	.2637
1.6	.0337	.1930	.2277	.2335	.2313	.2260
1.7	.0290	.1645	.1917	.1970	.1956	.1919
1.8	.0246	.1386	.1594	.1646	.1638	.1614
1.9	.0207	.1155	.1310	.1361	.1358	.1344
2.0	.0172	.0952	.1103	.1114	.1115	.1108
2.1	.0141	.0776	.0889	.0903	.0906	.0903
2.2	.0114	.0626	.0708	.0724	.0729	.0728
2.3	.0092	.0500	.0582	.0575	.0580	.0580
2.4	.0073	.0395	.0455	.0452	.0457	.0457
2.5	.0057	.0310	.0353	.0351	.0355	.0356
2.6	.0045	.0240	.0271	.0270	.0273	.0273
2.7	.0035	.0185	.0217	.0206	.0208	.0208
2.8	.0027	.0142	.0165	.0156	.0156	.0156
2.9	.0020	.0108	.0125	.0117	.0116	.0115
3.0	.0015	.0082	.0099	.0087	.0085	.0084
3.1	.0012	.0062	.0074	.0065	.0062	.0061
3.2	.0009	.0047	.0056	.0049	.0046	.0045
3.3	.0007	.0036	.0043	.0037	.0034	.0034
3.4	.0005	.0028	.0034	.0029	.0027	.0029
3.5	.0004	.0022	.0026	.0024	.0022	.0027

TABLE 2

AXIAL VELOCITY W OF VORTEX FLOWS

$\frac{r_0 A}{\sigma}$	.1923	1.204	1.523	1.767	1.857	1.951
η \ R	1	10	20	50	100	500
0	.0000	.0000	.0000	.0000	.0000	.0000
.1	-.0087	-.0102	-.0131	-.0153	-.0187	-.0263
.2	-.0312	-.0355	-.0433	-.0471	-.0519	-.0456
.3	-.0618	-.0681	-.0787	-.0794	-.0787	-.0454
.4	-.0950	-.1009	-.1053	-.1029	-.0917	-.0372
.5	-.1258	-.1284	-.1280	-.1134	-.0900	-.0238
.6	-.1499	-.1463	-.1366	-.1094	-.0748	-.0035
.7	-.1638	-.1516	-.1327	-.0912	-.0476	+.0252
.8	-.1651	-.1429	-.1128	-.0599	-.0102	.0623
.9	-.1525	-.1197	-.0776	-.0169	+.0360	.1067
1.0	-.1256	-.0827	-.0287	+.0358	.0894	.1573
1.1	-.0851	-.0332	+.0209	.0965	.1487	.2126
1.2	-.0322	+.0269	.0889	.1629	.2122	.2714
1.3	+.0311	.0952	.1508	.2332	.2784	.3323
1.4	.1024	.1695	.2290	.3054	.3460	.3940
1.5	.1793	.2472	.3091	.3777	.4133	.4554
1.6	.2592	.3261	.3756	.4486	.4793	.5154
1.7	.3398	.4040	.4535	.5167	.5427	.5731
1.8	.4190	.4792	.5276	.5809	.6026	.6278
1.9	.4949	.5502	.5966	.6406	.6584	.6791
2.0	.5661	.6160	.6496	.6950	.7095	.7264
2.1	.6317	.6759	.7073	.7440	.7556	.7696
2.2	.6910	.7294	.7583	.7875	.7966	.8082
2.3	.7436	.7765	.7957	.8255	.8326	.8424
2.4	.7896	.8173	.8346	.8582	.8639	.8721
2.5	.8291	.8522	.8675	.8861	.8905	.8975
2.6	.8626	.8814	.8948	.9094	.9130	.9190
2.7	.8906	.9057	.9138	.9287	.9317	.9369
2.8	.9136	.9256	.9325	.9444	.9471	.9516
2.9	.9323	.9416	.9476	.9570	.9594	.9635
3.0	.9474	.9543	.9576	.9668	.9692	.9729
3.1	.9593	.9643	.9673	.9744	.9767	.9801
3.2	.9686	.9721	.9748	.9802	.9823	.9853
3.3	.9758	.9780	.9806	.9844	.9863	.9887
3.4	.9813	.9825	.9845	.9875	.9890	.9906
3.5	.9854	.9859	.9882	.9896	.9908	.9913

TABLE 3

PRESSURE DISTRIBUTION P OF VORTEX FLOWS

η \ R	1	10	20	50	100	500
0	.9992	.9585	.9172	.8528	.8027	.7141
.1	.9992	.9585	.9170	.8526	.8023	.7130
.2	.9992	.9580	.9158	.8504	.7989	.7075
.3	.9992	.9563	.9118	.8442	.7909	.7004
.4	.9991	.9528	.9058	.8340	.7794	.6942
.5	.9990	.9474	.8959	.8210	.7669	.6897
.6	.9988	.9405	.8860	.8076	.7558	.6877
.7	.9986	.9328	.8739	.7957	.7480	.6890
.8	.9984	.9252	.8631	.7872	.7444	.6942
.9	.9982	.9186	.8550	.7830	.7457	.7036
1.0	.9980	.9137	.8508	.7838	.7519	.7170
1.1	.9979	.9111	.8505	.7895	.7626	.7339
1.2	.9979	.9109	.8540	.7995	.7771	.7538
1.3	.9979	.9131	.8598	.8131	.7945	.7756
1.4	.9979	.9174	.8696	.8293	.8140	.7987
1.5	.9980	.9234	.8816	.8471	.8346	.8222
1.6	.9982	.9305	.8927	.8655	.8553	.8453
1.7	.9984	.9384	.9066	.8838	.8755	.8674
1.8	.9985	.9464	.9203	.9013	.8946	.8880
1.9	.9987	.9543	.9333	.9175	.9120	.9068
2.0	.9989	.9616	.9433	.9320	.9277	.9235
2.1	.9991	.9683	.9541	.9448	.9414	.9381
2.2	.9993	.9742	.9634	.9558	.9531	.9506
2.3	.9994	.9793	.9701	.9650	.9630	.9611
2.4	.9995	.9836	.9768	.9726	.9711	.9697
2.5	.9996	.9871	.9823	.9787	.9777	.9767
2.6	.9997	.9900	.9866	.9836	.9829	.9823
2.7	.9998	.9923	.9896	.9875	.9870	.9866
2.8	.9998	.9940	.9924	.9905	.9902	.9899
2.9	.9999	.9954	.9945	.9927	.9926	.9924
3.0	.9999	.9965	.9959	.9944	.9944	.9943
3.1	.9999	.9973	.9973	.9957	.9957	.9957
3.2	1.0000	.9980	.9983	.9967	.9967	.9967
3.3		.9985	.9990	.9975	.9974	.9974
3.4		.9988	.9995	.9980	.9979	.9980
3.5		.9991	1.0000	.9985	.9984	.9985

TABLE 4

RADIAL VELOCITY U OF VON KÁRMÁN FLOWS

η \ R	.1	1	10	50	100
0	.0000	.0000	.0000	.0000	.0000
.05	.5114-3	.5105-2	.4469-1	.1147	.1464
.10	.8142-3	.8125-2	.6940-1	.1512	.1657
.15	.9527-3	.9504-2	.7916-1	.1456	.1360
.20	.9710-3	.9683-2	.7860-1	.1218	.0962
.25	.9088-3	.9060-2	.7166-1	.0935	.0618
.30	.7998-3	.7971-2	.6143-1	.0676	.0366
.35	.6702-3	.6678-2	.5015-1	.0467	.0199
.40	.5388-3	.5366-2	.3929-1	.0311	.0098
.45	.4175-3	.4157-2	.2968-1	.0200	.0043
.50	.3129-3	.3114-2	.2169-1	.0125	.0015
.55	.2272-3	.2261-2	.1537-1	.0076	
.60	.1603-3	.1594-2	.1059-1	.0045	
.65	.1099-3	.1093-2	.0709-1	.0026	
.70	.0733-3	.0729-2	.0462-1	.0015	
.75	.0477-3	.0474-2	.0294-1	.0008	
.80	.0302-3	.0300-2	.1082-1	.0004	
.85	.0186-3	.0185-2	.0110-1	.0002	
.90	.0112-3	.0112-2	.0065-1	.0001	
.95	.0066-3	.0066-2	.0037-1	.0001	
1.00	.0038-3	.0038-2	.0021-1		
1.05	.0021-3	.0021-2	.0012-1		
1.10	.0012-3	.0012-2	.0006-1		
1.15	.0006-3	.0006-2	.0003-1		
1.20	.0003-3	.0003-2	.0002-1		
1.25	.0002-3	.0002-2	.0001-1		
1.30	.0001-3	.0001-2	.0001-1		

TABLE 5

TANGENTIAL VELOCITY V OF VON KÁRMÁN FLOWS

η \ R	.1	1	10	50	100
0	1.0000	1.0000	1.0000	1.0000	1.0000
.05	.8875	.8873	.8713	.7776	.7006
.10	.7773	.7769	.7470	.5833	.4647
.15	.6714	.6708	.6306	.4263	.2990
.20	.5716	.5710	.5243	.3050	.1889
.25	.4795	.4788	.4291	.2143	.1177
.30	.3961	.3955	.3458	.1479	.0719
.35	.3222	.3215	.2743	.1003	.0425
.40	.2579	.2573	.2141	.0668	.0235
.45	.2031	.2025	.1644	.0438	.0112
.50	.1573	.1568	.1241	.0281	.0035
.55	.1198	.1194	.0921	.0178	
.60	.0897	.0894	.0672	.0110	
.65	.0660	.0657	.0481	.0067	
.70	.0477	.0475	.0339	.0040	
.75	.0339	.0337	.0234	.0023	
.80	.0237	.0235	.0159	.0014	
.85	.0162	.0161	.0106	.0008	
.90	.0109	.0108	.0070	.0004	
.95	.0072	.0072	.0045	.0002	
1.00	.0047	.0046	.0028	.0001	
1.05	.0030	.0030	.0018	.0001	
1.10	.0019	.0018	.0011		
1.15	.0011	.0011	.0006		
1.20	.0007	.0007	.0004		
1.25	.0004	.0004	.0002		
1.30	.0002	.0002	.0001		

TABLE 6

AXIAL VELOCITY W OF VON KÁRMÁN FLOWS

$\frac{w_\infty}{a\omega}$	-.7643-3	-.7618-2	-.5954-1	-.8366-1	-.6987-1
η \ R	.1	1	10	50	100
0	.0000	.0000	.0000	.0000	.0000
.05	.0360	.0360	.0407	.0785	.1264
.10	.1247	.1249	.1389	.2432	.3592
.15	.2419	.2421	.2654	.4234	.5780
.20	.3688	.3692	.3990	.5842	.7442
.25	.4924	.4929	.5259	.7129	.8562
.30	.6045	.6050	.6379	.8088	.9255
.35	.7008	.7012	.7316	.8766	.9650
.40	.7799	.7802	.8066	.9226	.9856
.45	.8423	.8426	.8643	.9527	.9953
.50	.8898	.8901	.9072	.9718	.9992
.55	.9250	.9251	.9381	.9836	
.60	.9501	.9503	.9597	.9907	
.65	.9676	.9677	.9744	.9948	
.70	.9795	.9795	.9841	.9972	
.75	.9873	.9873	.9903	.9985	
.80	.9923	.9923	.9943	.9992	
.85	.9954	.9955	.9967	.9996	
.90	.9974	.9974	.9981	.9998	
.95	.9985	.9985	.9990	.9999	
1.00	.9992	.9992	.9994	1.0000	
1.05	.9996	.9996	.9997		
1.10	.9998	.9998	.9998		
1.15	.9999	.9999	.9999		
1.20	.9999	.9999	1.0000		
1.25	1.0000	1.0000			

TABLE 7

PRESSURE DISTRIBUTION P OF VON KÁRMÁN FLOWS

η \ R	.1	1	10	50	100
0	-.2946+5	-.2954+3	-3.594	-.3793	-.1768
.05	+.5683+4	+.5773+2	+1.468	+.9429	+1.043
.10	.2713+5	.2730+3	4.375	1.437	1.335
.15	.3815+5	.3836+3	5.740	1.537	1.328
.20	.4173+5	.4194+3	6.080	1.480	1.255
.25	.4038+5	.4057+3	5.797	1.379	1.180
.30	.3614+5	.3631+3	5.186	1.279	1.118
.35	.3053+5	.3069+3	4.450	1.196	1.071
.40	.2463+5	.2476+3	3.716	1.133	1.038
.45	.1909+5	.1921+3	3.057	1.087	1.016
.50	.1429+5	.1440+3	2.505	1.056	1.003
.55	.1035+5	.1046+3	2.067	1.034	
.60	.7275+4	.7377+2	1.734	1.021	
.65	.4969+4	.5068+2	1.491	1.012	
.70	.3301+4	.3395+2	1.320	1.007	
.75	.2135+4	.2232+2	1.203	1.004	
.80	.1344+4	.1442+2	1.125	1.002	
.85	.8244+3	.9226+1	1.075	1.001	
.90	.4924+3	.5908+1	1.044	1.001	
.95	.2862+3	.3848+1	1.025	1.000	
1.00	.1616+3	.2603+1	1.014		
1.05	.8830+2	.1872+1	1.007		
1.10	.4646+2	.1453+1	1.004		
1.15	.2318+2	.1221+1	1.002		
1.20	.1065+2	.1096+1	1.001		
1.25	.4218+1	.1032+1	1.000		
1.30	.1000+1	.1000+1			

TABLE 8

RADIAL VELOCITY $\ddot{U}$ OF BODEWADT FLOWS

η \ R	.1	1	5	8
0	.0000	.0000	.0000	.0000
.05	.1165-2	.1165-1	.0582	.0907
.10	.2054-2	.2054-1	.1025	.1594
.15	.2662-2	.2663-1	.1329	.2059
.20	.3004-2	.3004-1	.1500	.2316
.25	.3111-2	.3112-1	.1554	.2391
.30	.3028-2	.3029-1	.1514	.2320
.35	.2804-2	.2806-1	.1403	.2141
.40	.2490-2	.2491-1	.1247	.1895
.45	.2129-2	.2130-1	.1068	.1615
.50	.1759-2	.1760-1	.0884	.1329
.55	.1407-2	.1409-1	.0709	.1059
.60	.1092-2	.1094-1	.0551	.0818
.65	.0824-2	.0825-1	.0417	.0613
.70	.0604-2	.0605-1	.0306	.0447
.75	.0431-2	.0432-1	.0219	.0317
.80	.0300-2	.0300-1	.0153	.0218
.85	.0203-2	.0204-1	.0104	.0147
.90	.0134-2	.0135-1	.0069	.0095
.95	.0087-2	.0087-1	.0045	.0061
1.00	.0055-2	.0055-1	.0028	.0037
1.05	.0034-2	.0034-1	.0017	.0023
1.10	.0020-2	.0020-1	.0011	.0013
1.15	.0012-2	.0012-1	.0006	.0008
1.20	.0007-2	.0007-1	.0004	.0004
1.25	.0004-2	.0004-1	.0002	.0002
1.30	.0002-2	.0002-1	.0001	.0001

TABLE 9

TANGENTIAL VELOCITY V OF BODEWADT FLOWS

η \ R	• .1	1	5	8
0	.0000	.0000	.0000	.0000
.05	.1125	.1126	.1173	.1261
.10	.2227	.2230	.2321	.2496
.15	.3286	.3291	.3422	.3674
.20	.4284	.4290	.4453	.4770
.25	.5205	.5212	.5399	.5763
.30	.6039	.6046	.6246	.6639
.35	.6778	.6785	.6987	.7390
.40	.7421	.7428	.7623	.8017
.45	.7969	.7975	.8156	.8527
.50	.8427	.8433	.8593	.8930
.55	.8802	.8807	.8944	.9241
.60	.9103	.9107	.9221	.9473
.65	.9340	.9343	.9435	.9643
.70	.9523	.9525	.9596	.9764
.75	.9661	.9663	.9716	.9847
.80	.9763	.9765	.9804	.9904
.85	.9838	.9839	.9867	.9941
.90	.9891	.9891	.9911	.9965
.95	.9928	.9928	.9941	.9979
1.00	.9953	.9953	.9962	.9988
1.05	.9970	.9970	.9976	.9994
1.10	.9981	.9981	.9985	.9997
1.15	.9989	.9989	.9991	.9998
1.20	.9993	.9993	.9994	.9999
1.25	.9996	.9996	.9997	1.0000
1.30	.9998	.9998	.9998	

TABLE 10

AXIAL VELOCITY W OF BÖDEWADT FLOWS

$\frac{w_\infty}{\alpha\omega}$	.2953-2	.2955-1	1.480	.2251
η \ R	.1	1	5	8
.00	.0000	.0000	.0000	.0000
.05	.0205	.0205	.0204	.0209
.10	.0758	.0758	.0755	.0773
.15	.1564	.1564	.1558	.1592
.20	.2531	.2530	.2520	.2571
.25	.3572	.3571	.3558	.3622
.30	.4616	.4615	.4599	.4673
.35	.5607	.5605	.5587	.5667
.40	.6505	.6504	.6485	.6565
.45	.7288	.7286	.7268	.7346
.50	.7946	.7945	.7927	.7999
.55	.8481	.8480	.8464	.8528
.60	.8903	.8902	.8889	.8944
.65	.9226	.9226	.9214	.9260
.70	.9467	.9466	.9457	.9495
.75	.9641	.9640	.9633	.9663
.80	.9763	.9763	.9758	.9780
.85	.9848	.9848	.9844	.9861
.90	.9904	.9904	.9902	.9914
.95	.9941	.9941	.9939	.9948
1.00	.9965	.9965	.9964	.9969
1.05	.9980	.9979	.9979	.9982
1.10	.9989	.9988	.9988	.9990
1.15	.9994	.9994	.9994	.9994
1.20	.9997	.9997	.9997	.9997
1.25	.9999	.9999	.9999	.9998
1.30	1.0000	1.0000	1.0000	.9999

TABLE 11

PRESSURE DISTRIBUTION P OF BODEWADT FLOWS

η \ R	.1	1	5	8
0	+.9398+4	+.9396+2	3.762	+1.525
.05	+.4034+4	+.4038+2	1.631	+ .6278
.10	-.1593+3	-.1522+1	- .0300	- .0648
.15	-.3222+4	-.3211+2	-1.229	- .5501
.20	-.5248+4	-.5231+2	-1.996	- .8388
.25	-.6376+4	-.6352+2	-2.383	- .9529
.30	-.6773+4	-.6741+2	-2.461	- .9239
.35	-.6619+4	-.6579+2	-2.304	- .7886
.40	-.6087+4	-.6037+2	-1.990	- .5849
.45	-.5331+4	-.5272+2	-1.587	- .3469
.50	-.4478+4	-.4412+2	-1.152	- .1025
.55	-.3626+4	-.3551+2	- .7269	+ .1290
.60	-.2838+4	-.2757+2	- .3435	+ .3333
.65	-.2151+4	-.2066+2	- .0127	+ .5050
.70	-.1583+4	-.1493+2	+ .2588	+ .6431
.75	-.1131+4	-.1038+2	+ .4726	+ .7498
.80	-.7854+3	-.6902+1	+ .6350	+ .8294
.85	-.5262+3	-.4337+1	+ .7542	+ .8868
.90	-.3482+3	-.2504+1	+ .8390	+ .9269
.95	-.2221+3	-.1234+1	+ .8974	+ .9540
1.00	-.1362+3	-.3809	+ .9367	+ .9718
1.05	-.8073+2	+.1762	+ .9622	+ .9831
1.10	-.4569+2	+.5304	+ .9785	+ .9903
1.15	-.2395+2	+.7489	+ .9885	+ .9944
1.20	-.1093+2	+.8804	+ .9945	+ .9969
1.25	-.3312+1	+.9569	+ .9980	+ .9984
1.30	+.1000+1	+.1000+1	+1.000	+ .9991

TABLE 11

PRESSURE DISTRIBUTION P OF BODEWADT FLOWS

η \ R	.1	1	5	8
0	+.9398+4	+.9396+2	3.762	+1.525
.05	+.4034+4	+.4038+2	1.631	+ .6278
.10	-.1593+3	-.1522+1	- .0300	- .0648
.15	-.3222+4	-.3211+2	-1.229	- .5501
.20	-.5248+4	-.5231+2	-1.996	- .8388
.25	-.6376+4	-.6352+2	-2.383	- .9529
.30	-.6773+4	-.6741+2	-2.461	- .9239
.35	-.6619+4	-.6579+2	-2.304	- .7886
.40	-.6087+4	-.6037+2	-1.990	- .5849
.45	-.5331+4	-.5272+2	-1.587	- .3469
.50	-.4478+4	-.4412+2	-1.152	- .1025
.55	-.3626+4	-.3551+2	- .7269	+ .1290
.60	-.2838+4	-.2757+2	- .3435	+ .3333
.65	-.2151+4	-.2066+2	- .0127	+ .5050
.70	-.1583+4	-.1493+2	+ .2588	+ .6431
.75	-.1131+4	-.1038+2	+ .4726	+ .7498
.80	-.7854+3	-.6902+1	+ .6350	+ .8294
.85	-.5262+3	-.4337+1	+ .7542	+ .8868
.90	-.3482+3	-.2504+1	+ .8390	+ .9269
.95	-.2221+3	-.1234+1	+ .8974	+ .9540
1.00	-.1362+3	-.3809	+ .9367	+ .9718
1.05	-.8073+2	+.1762	+ .9622	+ .9831
1.10	-.4569+2	+.5304	+ .9785	+ .9903
1.15	-.2395+2	+.7489	+ .9885	+ .9944
1.20	-.1093+2	+.8804	+ .9945	+ .9969
1.25	-.3312+1	+.9569	+ .9980	+ .9984
1.30	+.1000+1	+.1000+1	+1.000	+ .9991

TABLE 12: COMPUTER OUTPUT FOR THE BÖDEWADT FLOW WITH R = 1 OBTAINED BY THE INTEGRAL EQUATION METHOD

η	G	G′	G″	V	V′
.00	.00000	.00000	.25919	.00000	.22602+1
.05	.3024-3	.1165-1	.2060	.1126	.2238+1
.10	.1119-2	.2055-1	.1496	.2230	.2171+1
.15	.2310-2	.2663-1	.9413-1	.3291	.2065+1
.20	.3738-2	.3004-1	.4361-1	.4290	.1925+1
.25	.5276-2	.3112-1	.8854-3	.5212	.1759+1
.30	.6818-2	.3029-1	-.3230-1	.6046	.1575+1
.35	.8281-2	.2806-1	-.5540-1	.6785	.1382+1
.40	.9608-2	.2491-1	-.6893-1	.7428	.1189+1
.45	.1076-1	.2130-1	-.7418-1	.7975	.1003+1
.50	.1174-1	.1760-1	-.7293-1	.8433	.8285
.55	.1253-1	.1409-1	-.6712-1	.8807	.6712
.60	.1315-1	.1094-1	-.5857-1	.9107	.5330
.65	.1363-1	.8248-2	-.4886-1	.9343	.4149
.70	.1398-1	.6050-2	-.3915-1	.9525	.3165
.75	.1424-1	.4319-2	-.3025-1	.9663	.2368
.80	.1442-1	.3004-2	-.2259-1	.9765	.1736
.85	.1455-1	.2037-2	-.1634-1	.9839	.1248
.90	.1463-1	.1347-2	-.1146-1	.9891	.8793-1
.95	.1469-1	.8699-3	-.7815-2	.9928	.6073-1
1.00	.1472-1	.5488-3	-.5181-2	.9953	.4112-1
1.05	.1474-1	.3386-3	-.3343-2	.9970	.2730-1
1.10	.1476-1	.2045-3	-.2102-2	.9981	.1776-1
1.15	.1476-1	.1212-3	-.1289-2	.9989	.1133-1
1.20	.1477-1	.7071-4	-.7721-3	.9993	.7084-2
1.25	.1477-1	.4077-4	-.4520-3	.9996	.4342-2
1.30	.1477-1	.2341-4	-.2592-3	.9998	.2609-2

TABLE 13 : COMPUTER OUTPUT FOR THE BÖDEWADT FLOW WITH R = 1 OBTAINED BY THE RUNGE-KUTTA METHOD

η	G	G′	G″	G‴	V	V′	V″
.00	.0000	.0000	.2592	-.1000+1	.0000	.2260+1	-.0000
.05	.3024-3	.1165-1	.2060	-.1111+1	.1126	.2238+1	-.8963
.10	.1119-2	.2055-1	.1496	-.1133+1	.2230	.2171+1	-.1741+1
.15	.2310-2	.2663-1	.9413-1	-.1071+1	.3291	.2065+1	-.2486+1
.20	.3737-2	.3004-1	.4361-1	-.9402	.4290	.1925+1	-.3092+1
.25	.5275-2	.3112-1	.8855-3	-.7628	.5212	.1759+1	-.3532+1
.30	.6818-2	.3029-1	-.3230-1	-.5627	.6046	.1575+1	-.3795+1
.35	.8281-2	.2806-1	-.5539-1	-.3630	.6785	.1382+1	-.3885+1
.40	.9608-2	.2491-1	-.6892-1	-.1824	.7428	.1189+1	-.3819+1
.45	.1076-1	.2130-1	-.7417-1	-.3367-1	.7975	.1003+1	-.3621+1
.50	.1174-1	.1760-1	-.7292-1	.7700-1	.8433	.8285	-.3324+1
.55	.1253-1	.1409-1	-.6711-1	.1492	.8807	.6712	-.2961+1
.60	.1315-1	.1094-1	-.5857-1	.1871	.9107	.5330	-.2564+1
.65	.1363-1	.8250-2	-.4886-1	.1974	.9343	.4149	-.2161+1
.70	.1399-1	.6051-2	-.3916-1	.1881	.9525	.3165	-.1775+1
.75	.1424-1	.4321-2	-.3025-1	.1666	.9663	.2368	-.1422+1
.80	.1442-1	.3005-2	-.2259-1	.1392	.9765	.1736	-.1112+1
.85	.1455-1	.2038-2	-.1635-1	.1109	.9839	.1248	-.8489
.90	.1463-1	.1348-2	-.1147-1	.8462-1	.9891	.8793-1	-.6332
.95	.1469-1	.8702-3	-.7819-2	.6214-1	.9928	.6073-1	-.4615
1.00	.1472-1	.5489-3	-.5183-2	.4404-1	.9953	.4112-1	-.3289
1.05	.1474-1	.3386-3	-.3344-2	.3019-1	.9970	.2730-1	-.2292
1.10	.1476-1	.2046-3	-.2103-2	.2005-1	.9981	.1776-1	-.1562
1.15	.1477-1	.1213-3	-.1289-2	.1293-1	.9989	.1133-1	-.1041
1.20	.1477-1	.7074-4	-.7717-3	.8098-2	.9993	.7084-2	-.6794-1
1.25	.1477-1	.4081-4	-.4516-3	.4936-2	.9996	.4342-2	-.4338-1
1.30	.1477-1	.2347-4	-.2589-3	.2930-2	.9998	.2609-2	-.2710-1
1.40	.1478-1	.8088-5	-.8105-4	.9584-3	.9999	.8870-3	-.9925-2
1.50	.1478-1	.3334-5	-.2500-4	.2871-3	1.0000	.2783-3	-.3338-2
1.60	.1478-1	.1818-5	-.8660-5	.8119-4	1.0000	.8052-4	-.1032-2
1.70	.1478-1	.1230-5	-.4030-5	.2374-4	1.0000	.2142-4	-.2931-3
1.80	.1478-1	.9125-6	-.2566-5	.8841-5	1.0000	.5187-5	-.7636-4
1.90	.1478-1	.6915-6	-.1916-5	.4970-5	1.0000	.1104-5	-.1814-4
2.00	.1478-1	.5222-6	-.1492-5	.3695-5	1.0000	.1741-6	-.3824-5

APPENDIX B

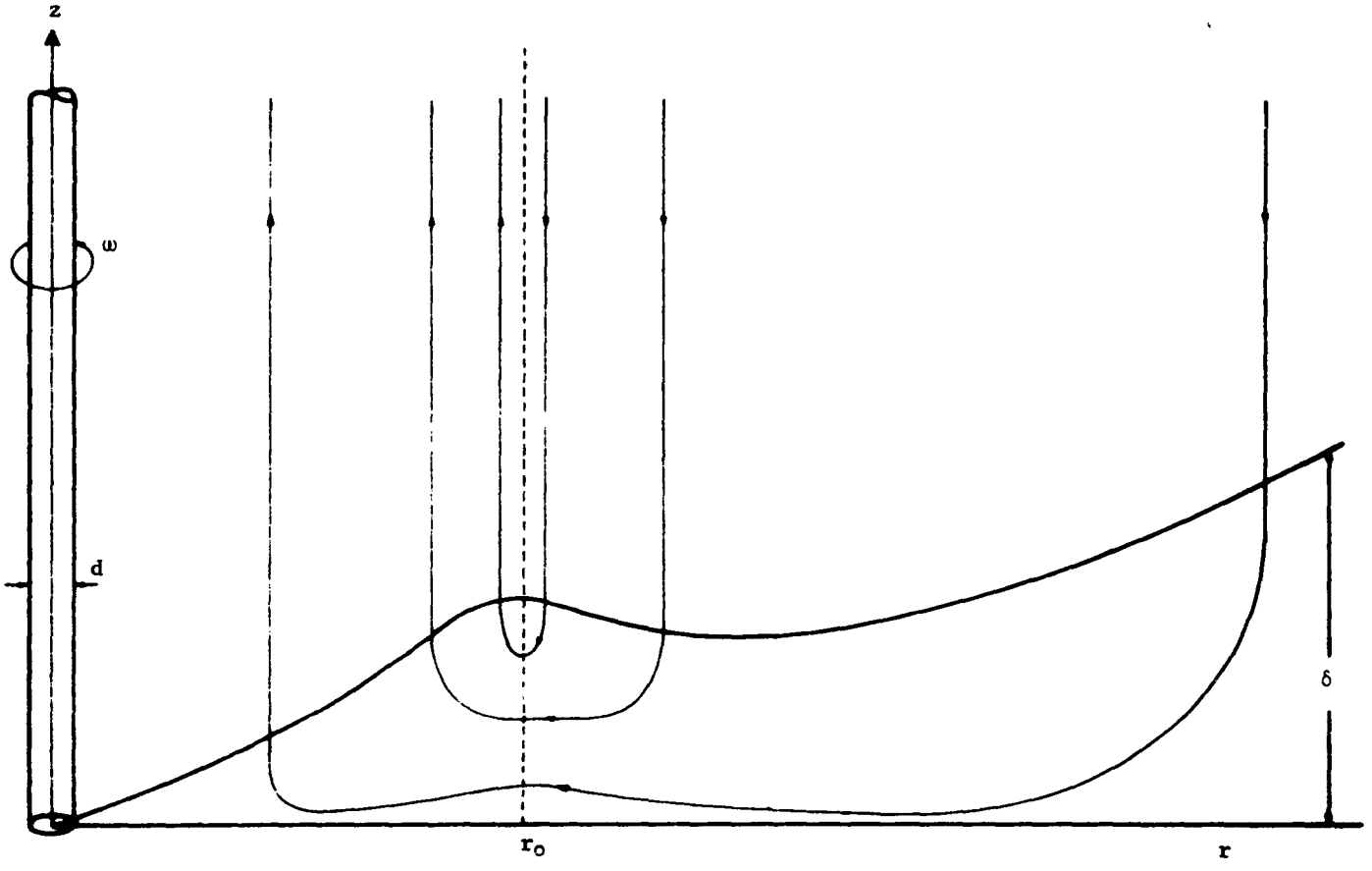

FIGURE 1 : Scheme of the secondary flow produced by a vortex motion normal to a flat surface.

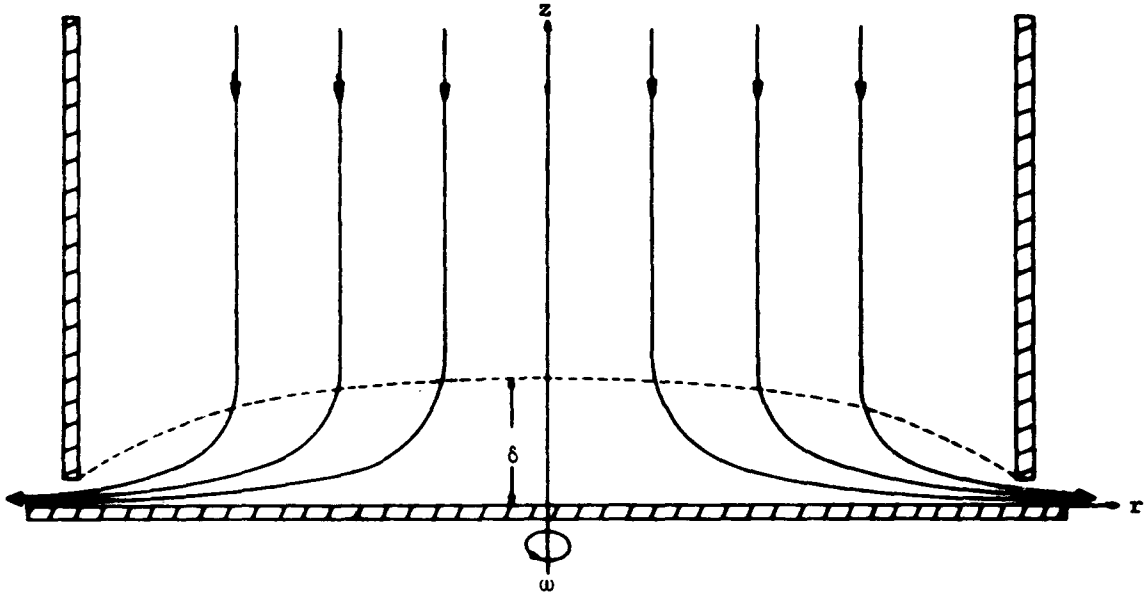

FIGURE 2: Scheme of the secondary flow produced by a rotating disk in a fluid at rest.

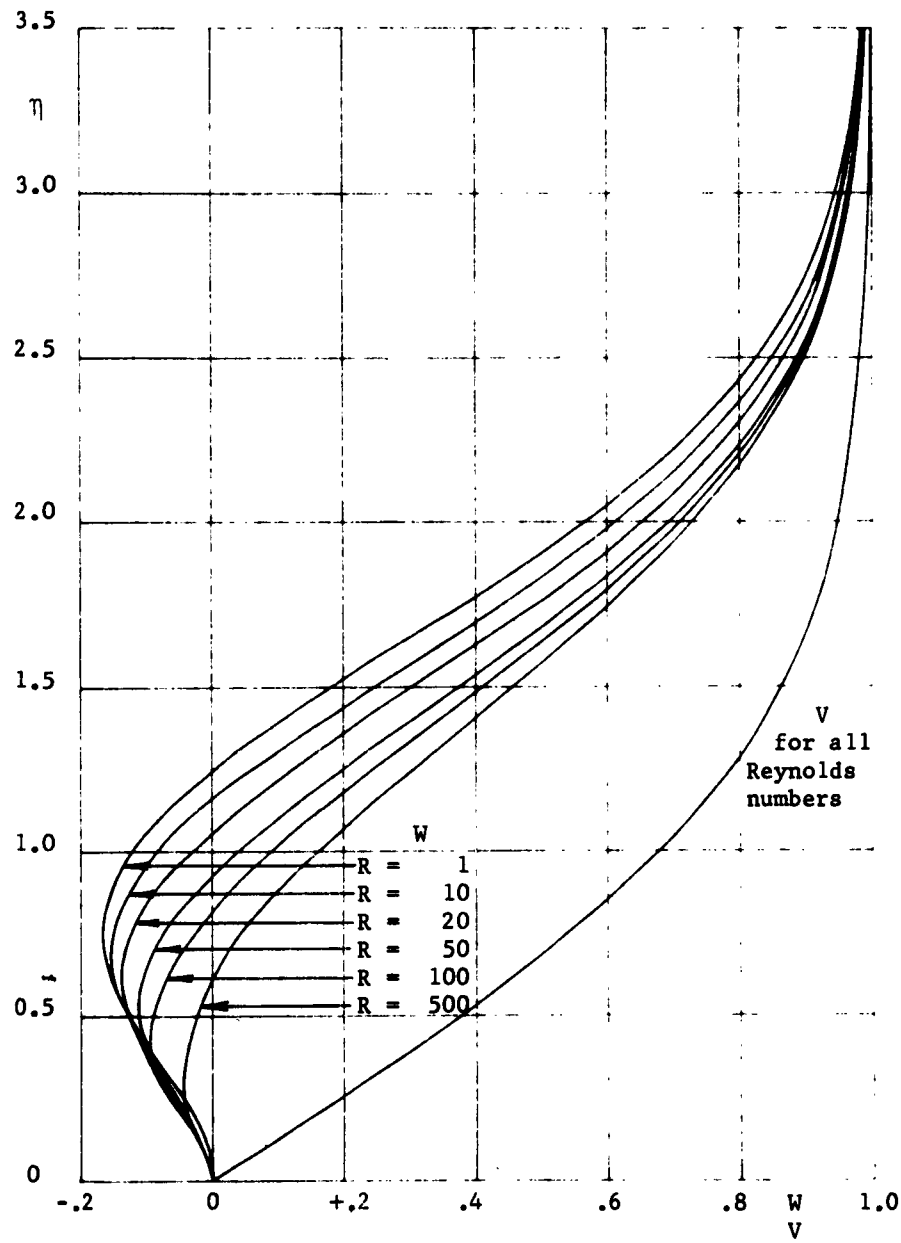

FIGURE 3: The dimensionless velocity components V and W vs. the dimensionless variable η for vortex flows.

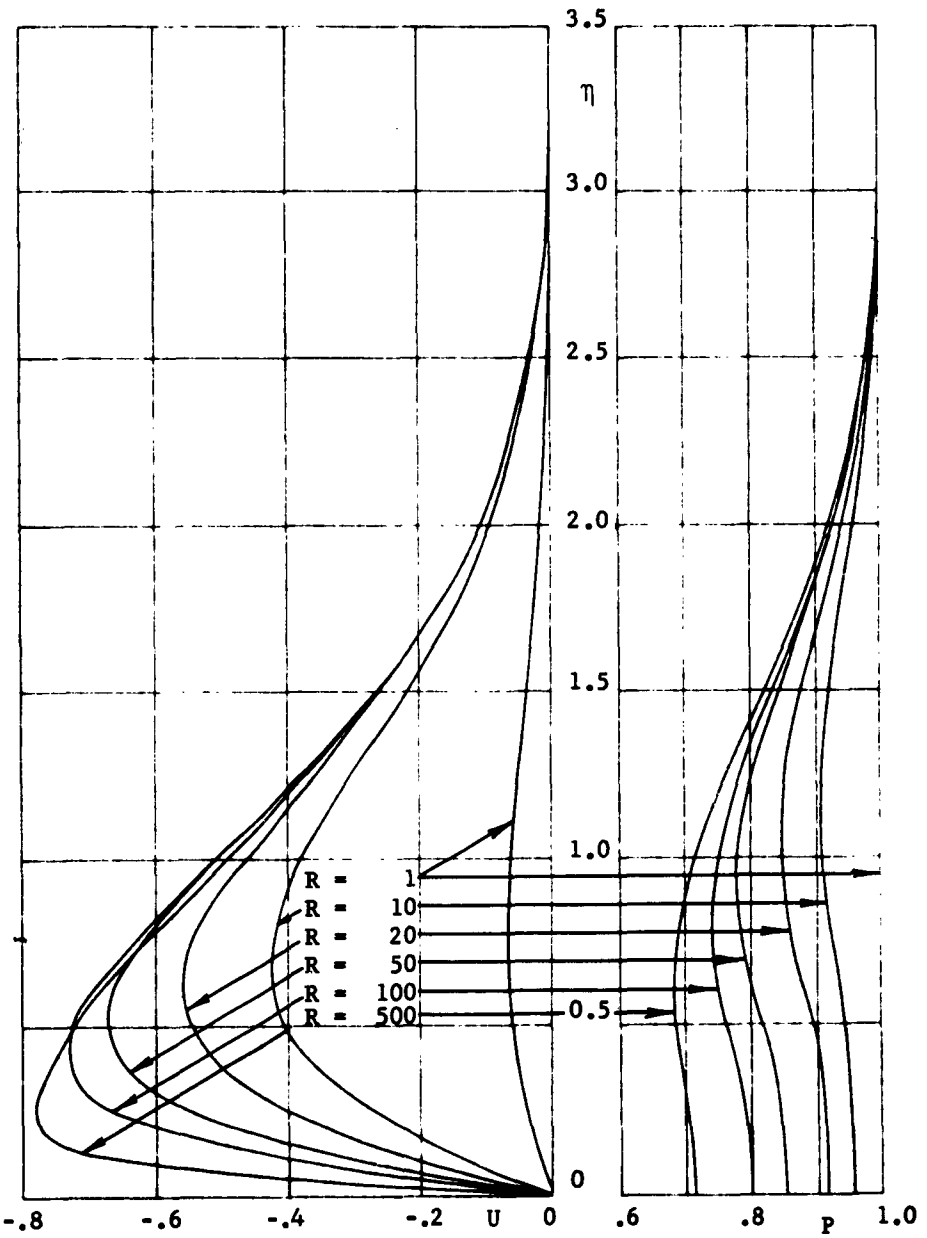

FIGURE 4: The dimensionless velocity component U vs. the dimensionless variable η for vortex flows.

FIGURE 5: The dimensionless pressure P vs. the dimensionless variable η for vortex flows.

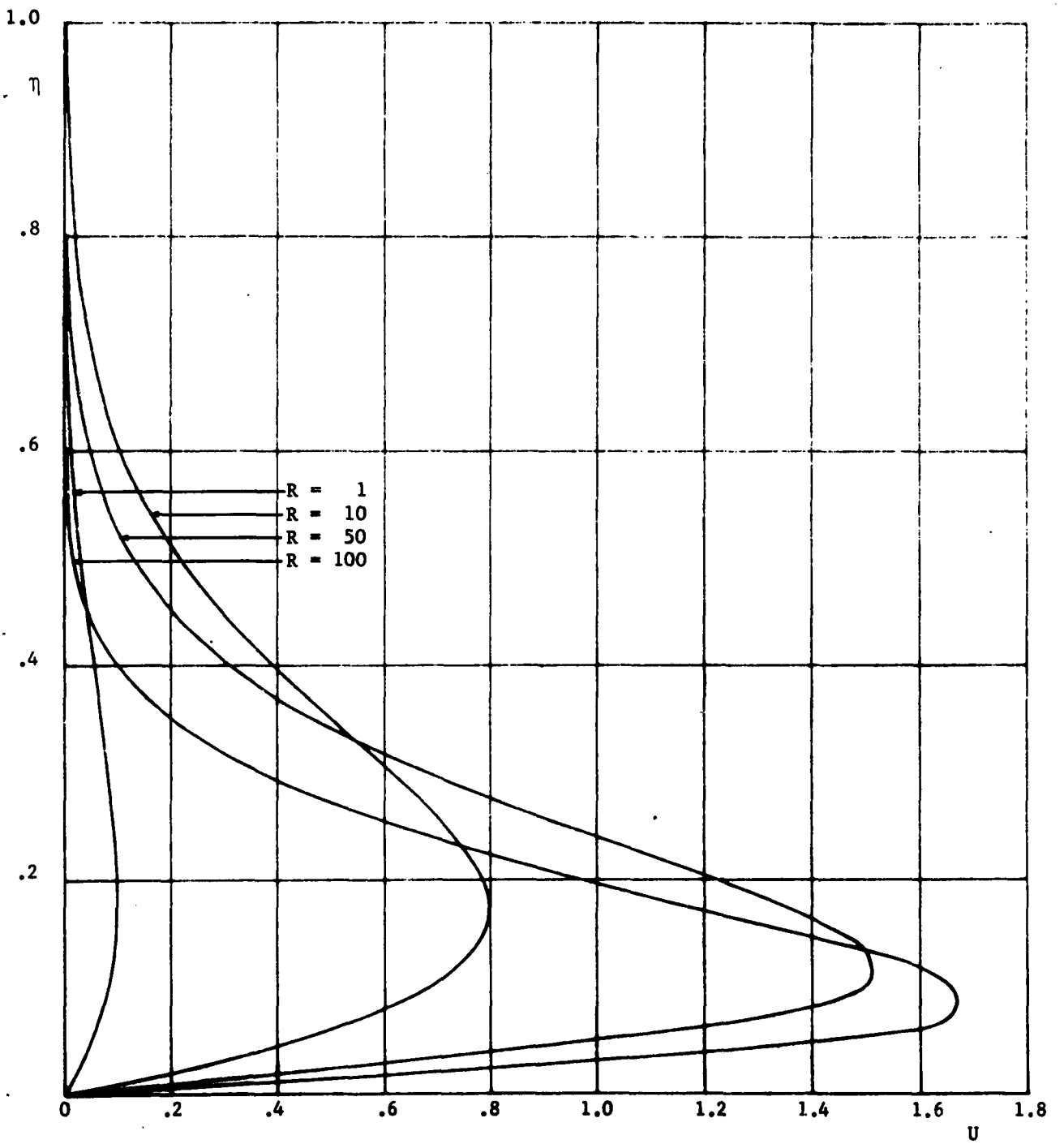

FIGURE 6: The dimensionless velocity component U vs. the dimensionless variable η for von Kármán flows.

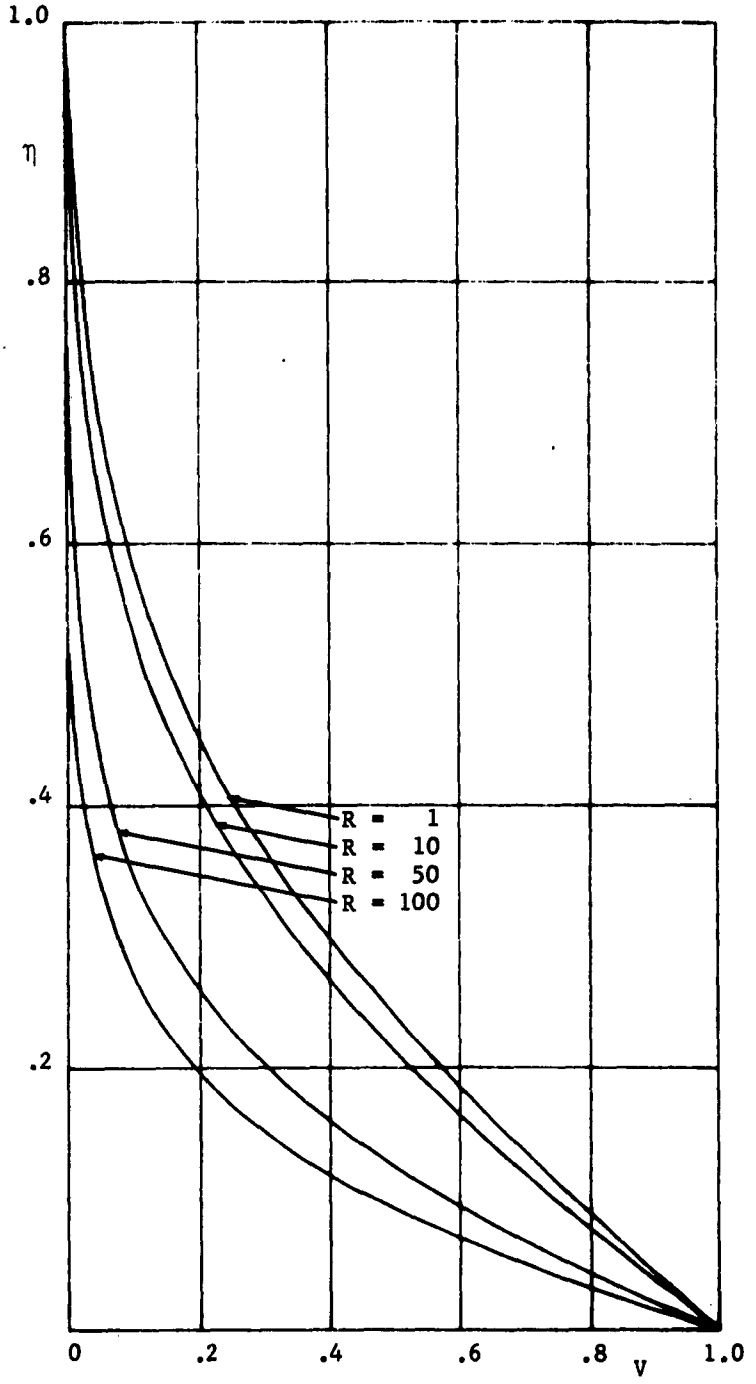

FIGURE 7: The dimensionless velocity component V vs. the dimensionless variable η for von Kármán flows.

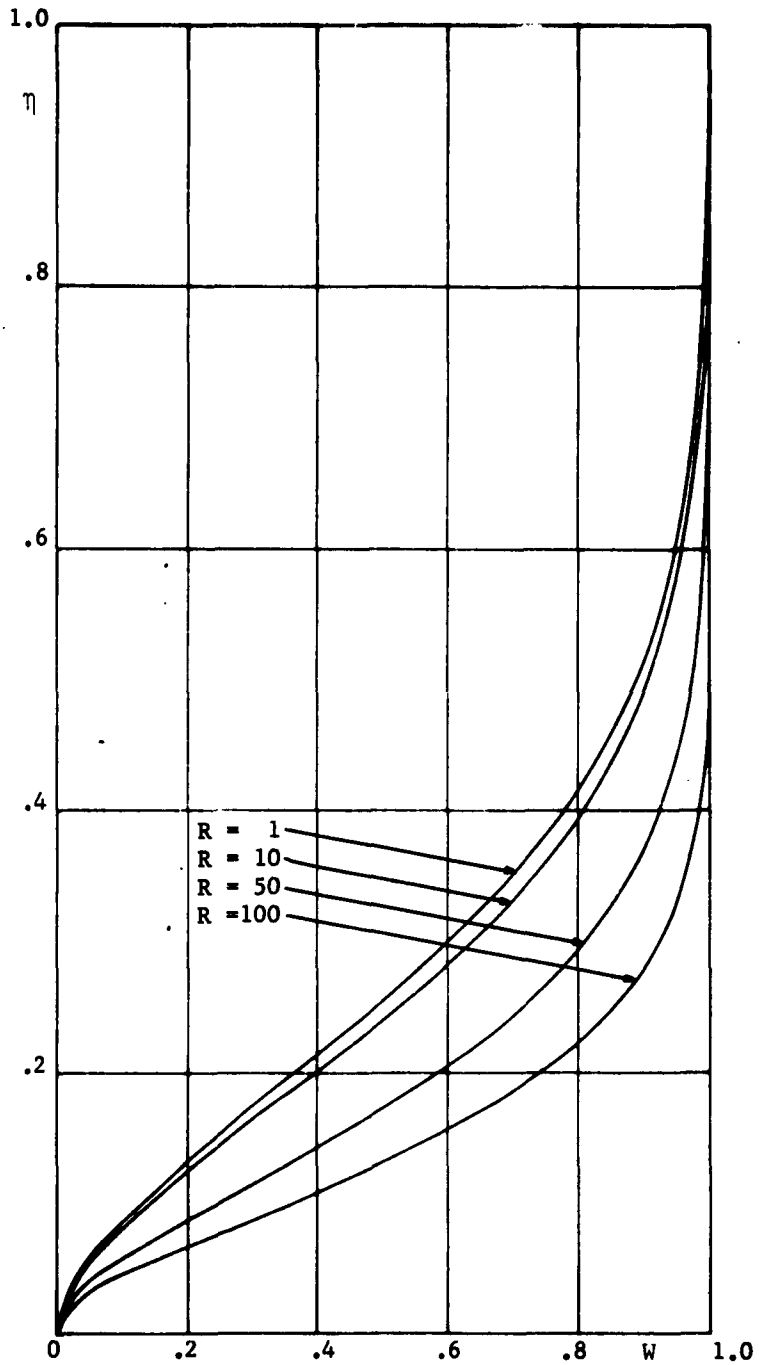

FIGURE 8 : The dimensionless velocity component W vs. the dimensionless variable η for von Kármán flows.

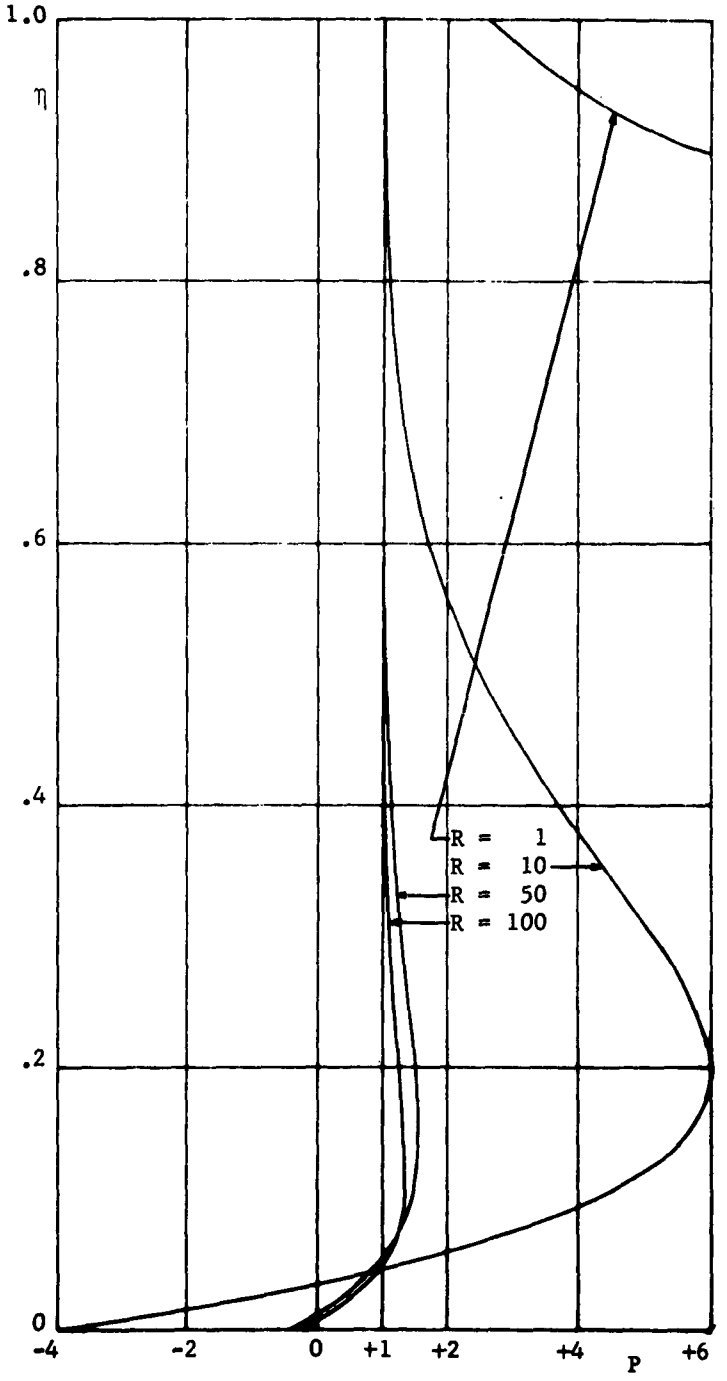

FIGURE 9: The dimensionless pressure P vs. the dimensionless variable η for von Kármán flows.

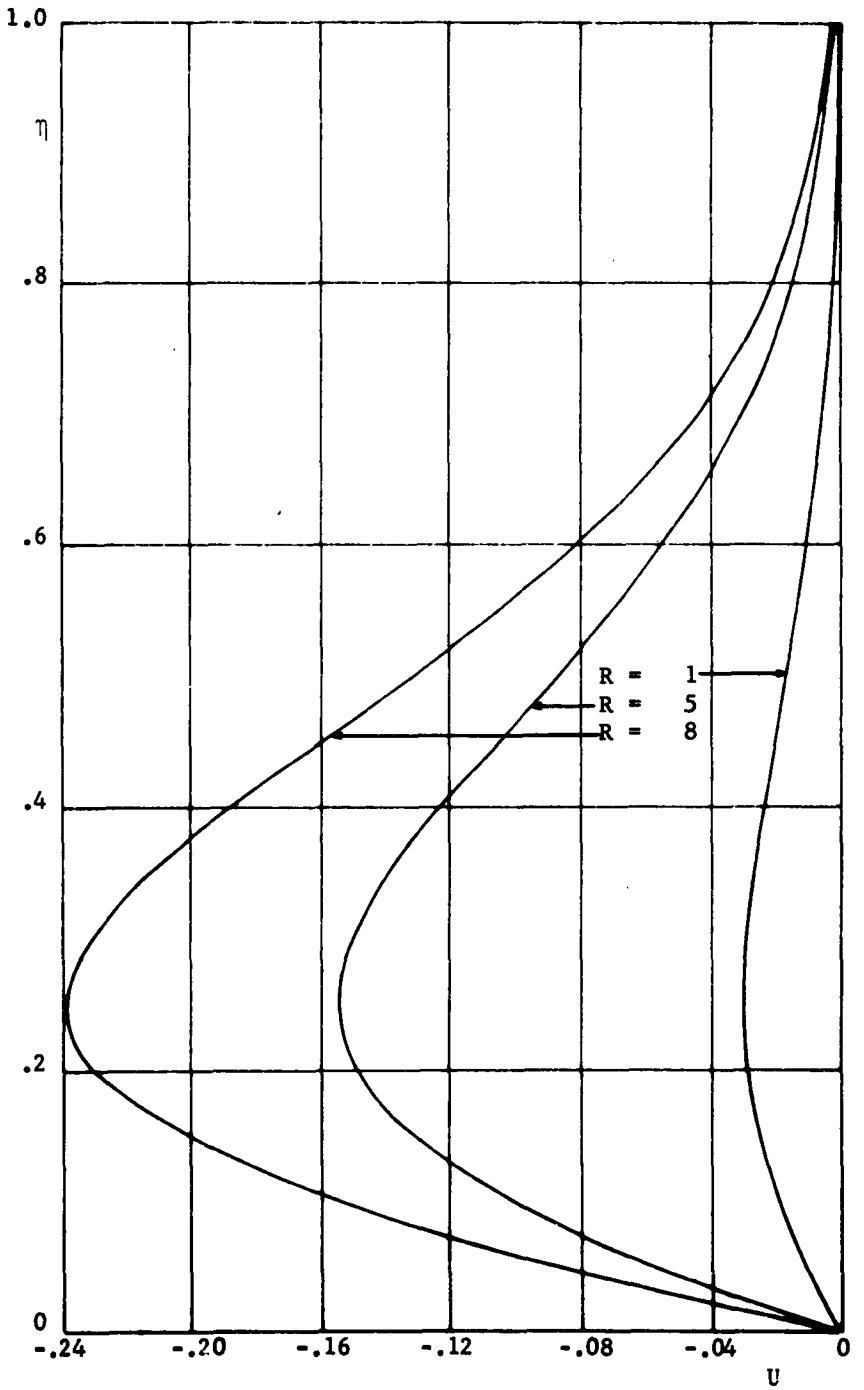

FIGURE 10 : The dimensionless velocity component U vs. the dimensionless variable η for Bödewadt flows.

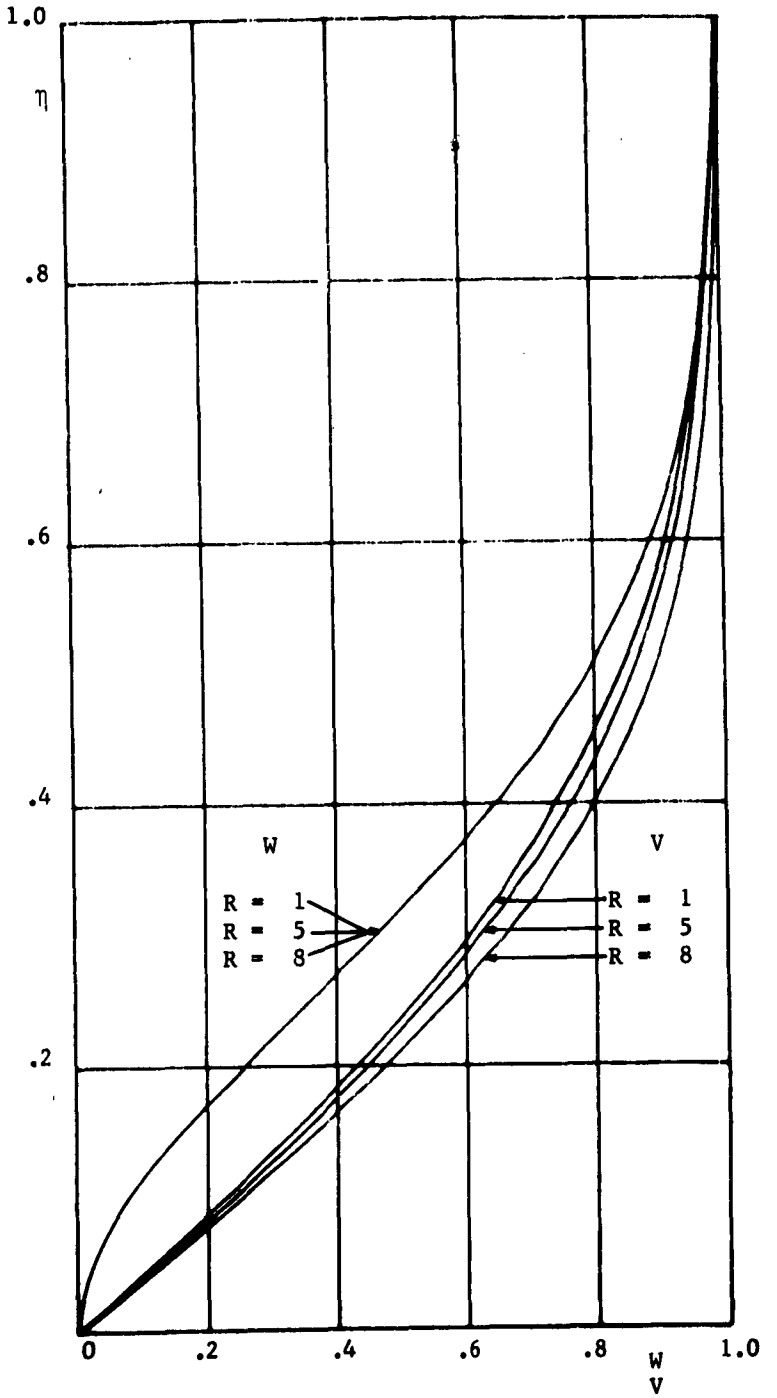

FIGURE 11: The dimensionless velocity components V and W vs. the dimensionless variable η for Bödewadt flows.

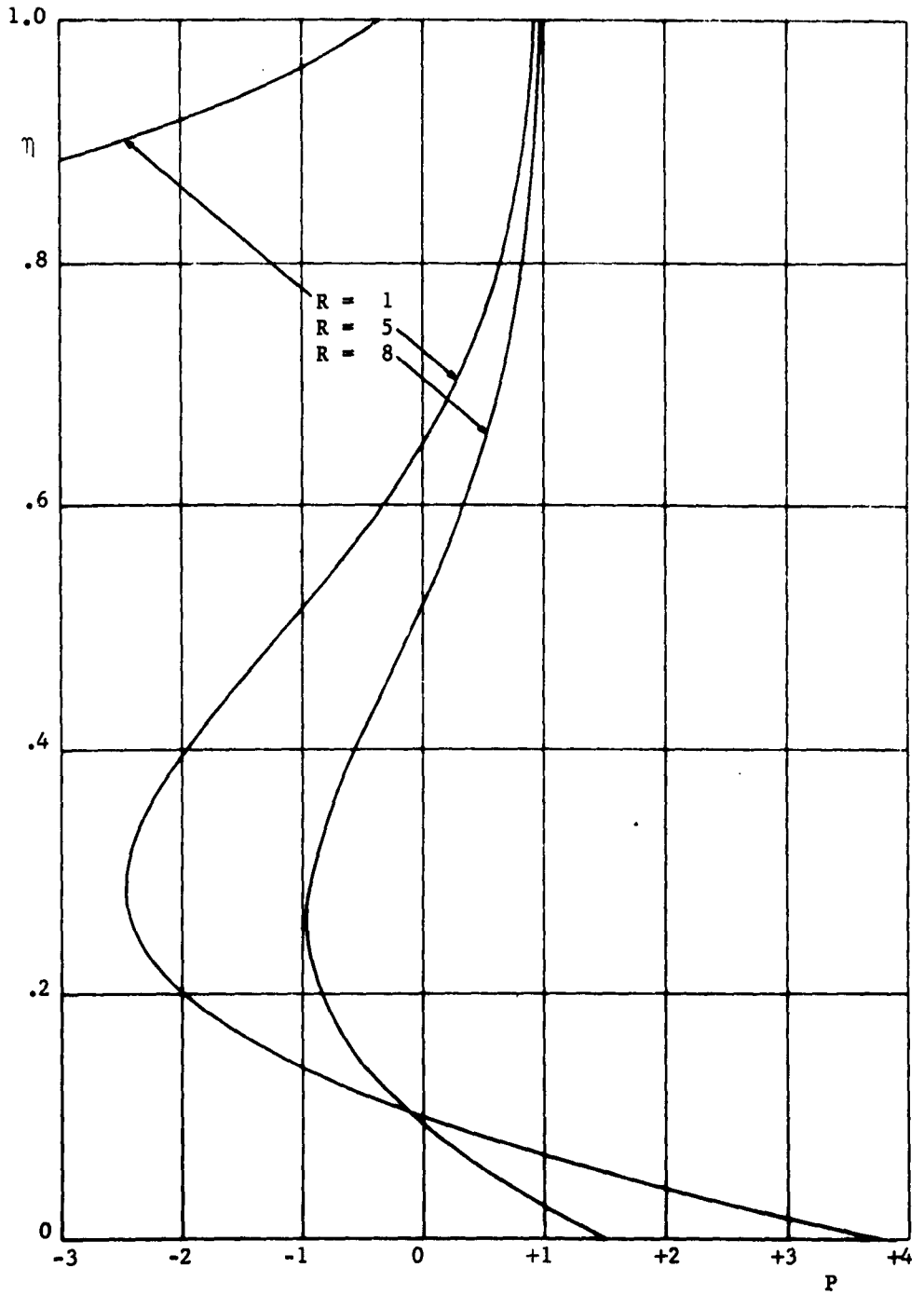

FIGURE 12: The dimensionless pressure P vs. the dimensionless variable η for Bödewadt flows.

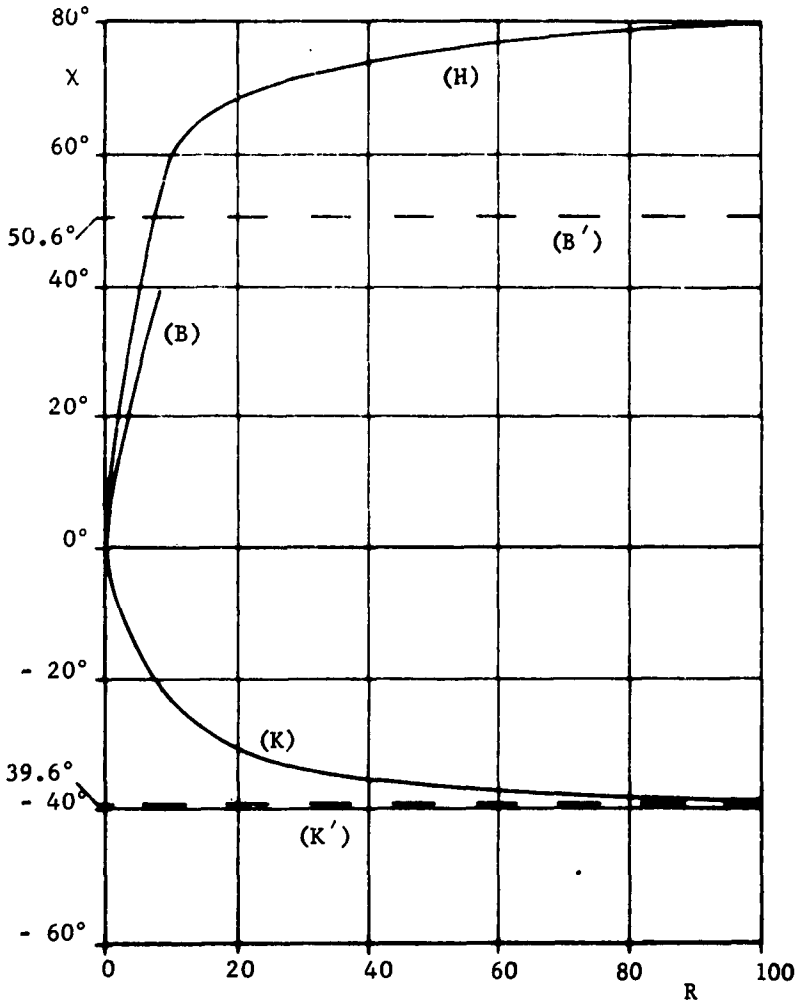

FIGURE 13 : The angle of deviation χ vs. the Reynolds numbers R.
(H): Vortex flows
(B): Bödewadt flows
(B′): Bödewadt's solution
(K): Von Kármán flows
(K′): Von Kármán's solution

APPENDIX C

DISTRIBUTION

Bureau of Naval Weapons

DLI-3	1
R-14	1
R-12	1
RREN	1
RRE	1
RT	1
RM	1

Special Projects Office
Department of the Navy
Washington 25, D. C.

SP-20	4
SP-43	2

Commander
Armed Services Technical Information Agency
Arlington Hall Station
Arlington 12, Virginia
Attn: TIPDR 10

Commanding General
Aberdeen Proving Ground
Aberdeen, Maryland
Attn: Technical Information Section
Development and Proof Services 2

Commander, Operational and Development Force
U. S. Atlantic Fleet, U. S. Naval Base
Norfolk 11, Virginia 1

Chief of Naval Research
Department of the Navy
Washington 25, D. C.

Attn: Code 438	2
Attn: Mathematical Sciences Division	1
Attn: Dr. F. J. Weyl	1
Attn: Mathematics Branch	1
Attn: Fluid Dynamics Branch	1

DISTRIBUTION (Continued)

Director Naval Research Laboratory Washington 25, D. C.	3
Commander Naval Ordnance Laboratory White Oak, Maryland	
Attn: Dr. R. Roberts	1
Attn: Dr. R. E. Wilson	2
Attn: Dr. A. VanTuyl	1
Attn: Technical Library	1
Chief, Bureau of Ships Department of the Navy Washington 25, D. C.	2
Director David Taylor Model Basin Washington 7, D. C.	
Attn: Dr. Daniel Shanks	1
Attn: Dr. John W. Wrench, Jr.	1
Attn: Dr. F. Frenkiel	1
Attn: Dr. H. Polachek	1
Attn: Dr. Elizabeth Cuthill	1
Attn: Library	2
Commander U. S. Naval Ordnance Test Station China Lake, California	
Attn: Dr. D. E. Zilmer	1
Attn: Library	2
Superintendent U. S. Naval Postgraduate School Monterey, California	
Attn: Library, Technical Reports Section	1
Director of the Institute of Naval Studies 185 Alewife Brook Parkway Cambridge 38, Massachusetts	1

DISTRIBUTION (Continued)

Commanding General
White Sands Proving Ground
La Cruces, New Mexico
Attn: Flight Determination Laboratory 1

Commander, 3206th Test Group
Building 100
Eglin Air Force Base, Florida
Attn: Mr. H. L. Adams 1

Commander
Wright Air Development Center
Wright-Patterson Air Force Base
Dayton, Ohio
Attn: WCRRN-4 1
Attn: Dr. K. G. Guderley 1

U. S. Atomic Energy Commission
Washington, D. C.
Attn: Technical Library 1

Los Alamos Scientific Laboratory
Los Alamos, New Mexico 2

Superintendent
U. S. Naval Academy
Annapolis, Maryland
Attn: Dept. of Mathematics 1
Attn: Library 1

U. S. Naval Observatory
Washington 25, D. C.
Attn: Dr. G. M. Clemence 1

U. S. Weather Bureau
Washington 25, D. C.
Attn: Dr. J. Smagorinsky 1

Commander
Naval Ordnance Test Station
Pasadena Annex
3202 Foothill Boulevard
Pasadena, California 1

DISTRIBUTION (Continued)

Army Rocket and Guided Missile Agency
U. S. Army Ordnance Missile Command
Redstone Arsenal, Alabama
Attn: Capt. Robert H. C. Au 1

National Aeronautics and Space Administration
1520 H Street, N. W.
Washington 25, D. C. 6

Commander
Ballistic Missile Division
ARDC P. O. Box 262
Inglewood, California
Attn: Col. Ebelke (WDTVR) 2

Commanding General
Army Ballistic Missile Agency
Redstone Arsenal
Huntsville, Alabama
Attn: Mr. H. G. Paul (ORDAB - DS) 1
Attn: Dr. W. Lucas (ORDAB - DS) 1
Attn: Mr. Dale L. Burrows (ORDAB - DSDA) 1
Attn: Technical Library 1

National Science Foundation
1520 H. Street, N. W.
Washington, D. C.
Attn: Engineering Sciences Division 1
Attn: Mathematical Sciences Division 1

Director
National Bureau of Standards
Washington 25, D. C.
Attn: Fluid Mechanics Division 1
Attn: Dr. G. B. Schubauer 1
Attn: Dr. G. H. Keulegan 1
Attn: Mr. J. H. Wegstein, Computation Laboratory 1
Attn: Dr. Phillip Davis 1
Attn: Dr. E. W. Cannon, Applied Mathematics Division 1
Attn: Dr. S. N. Alexander, Data Processing Division 1
Attn: Dr. R. J. Arms 1
Attn: Technical Library 1

DISTRIBUTION (Continued)

Office of Technical Services
Department of Commerce
Washington 25, D. C. 1

Guggenheim Aeronautical Laboratory
California Institute of Technology
Pasadena 4, California
Attn: Prof. Lester Lees 1
Attn: Prof. J. D. Cole 1

California Institute of Technology
Pasadena 4, California
Attn: Prof. John Todd 1

University of California
Berkeley 4, California
Attn: Prof. P. Lieber 1
Attn: Department of Mathematics 1

Institute of Mathematical Sciences
New York University
25 Waverly Place
New York 3, New York
Attn: Prof. J. J. Stoker 1
Attn: Prof. K. O. Friedrichs 1
Attn: Dr. Max Goldstein 1
Attn: Prof. B. Haurwitz 1
Attn: AEC Computing Facility 1

Harvard University
Cambridge 38, Massachusetts
Attn: Prof. G. Birkhoff 1
Attn: Division of Applied Sciences 1
Attn: Computation Laboratory 1
Attn: Prof. G. F. Carrier 1
Attn: Prof. H. M. Stommel 1

University of Maryland
College Park, Maryland
Attn: Prof. J. M. Burgers 1
Attn: Prof. J. Weske 1
Attn: Department of Mathematics 1
Attn: Institute for Fluid Dynamics and Applied Mathematics 1

DISTRIBUTION (Continued)

Massachusetts Institute of Technology
Cambridge, Mass.
Attn: Prof. C. C. Lin 1
Attn: Prof. A. H. Shapiro 1
Attn: Prof. J. G. Charney 1

The Johns Hopkins University
Baltimore 18, Maryland
Attn: Prof. R. R. Long 1

Applied Physics Laboratory
Johns Hopkins University
Silver Spring, Maryland
Attn: Librarian 2

University of California
San Diego, California
Attn: Prof. W. H. Munk 1

University of Chicago
Chicago, Illinois
Attn: Prof. H. Riehl 1

AVCO Manufacturing Corporation
Research and Advanced Development Division
201 Lowell Street
Wilmington, Massachusetts
Attn: J. P. Wamser
Via: INSMAT, Boston, Massachusetts 2

General Electric Co.
Missile and Space Vehicle Department
3198 Chestnut Street
Philadelphia 4, Pennsylvania
Attn: Mr. R. J. Kirby
Via: INSMAT, Philadelphia, Upper Darby, Pa. 2

Lewis Flight Propulsion Laboratory
National Aeronautics and Space Administration
Cleveland, Ohio
Attn: F. K. Moore 1
Attn: S. H. Maslen 1
Attn: W. E. Moeckel 1

DISTRIBUTION (Continued)

Lockheed Aircraft Corporation
Palo Alto, California
Attn: Dr. W. C. Griffith 1

Prof. M. Van Dyke
Department of Aeronautical Engineering
Stanford University
Stanford, California 1

Dr. Bernd Zondek
Computer Usage Company, Inc.
655 Madison Avenue
New York, New York 1

Prof. J. Siekmann
University of Florida
Gainesville, Florida 1

Dr. L. M. Mack
Jet Propulsion Laboratory
California Institute of Technology
Pasadena, California 1

Prof. W. D. Hayes
Department of Aeronautical Engineering
Princeton University
Princeton, N. J. 1

Prof. R. F. Probstein
Division of Engineering
Brown University
Providence 12, R. I. 1

Dr. C. C. Bramble
145 Monticello
Annapolis, Maryland 1

Dr. M. J. Lighthill
Royal Aircraft Establishment
Farnborough, Hampshire, England
Via: BUWEPS (DSC-3) 1

Prof. G. K. Batchelor
University of Cambridge
Cambridge, England
Via: BUWEPS (DSC-3) 1

DISTRIBUTION (Continued)

Prof. C. R. Illingworth University of Manchester Manchester, England Via: BUWEPS (DSC-3)	1
Prof. Dr. H. Goertler University of Freiburg Freiburg, Germany Via: BUWEPS (DSC-3)	1
Prof. Dr. H. Schlichting Technische Hochschule Braunschweig, Germany Via: BUWEPS (DSC-3)	1
Prof. Dr. W. Tollmien Max Planck Institute Goettingen, Germany Via: BUWEPS (DSC-3)	1
Prof. Dr. A. Naumann Technische Hochschule Aachen Aachen, Germany Via: BUWEPS (DSC-3)	1
Prof. Dr. J. Ackeret Eidgenoessische Technische Hochschule Zurich, Switzerland Via: BUWEPS (DSC-3)	1
Local:	
D	1
K	1
K-1	1
K-3	1
K-4	1
KXK	1
KXF	1
KXH	1
KYD	2
KXL	25
KYS	50
ACL	5
File	1

LIBRARY CATALOGING INPUT
PRNC-NWL-5070/15 (7-62)

BIBLIOGRAPHIC INFORMATION

DESCRIPTOR	CODE	DESCRIPTOR	CODE
SOURCE Naval Weapons Laboratory	NPGA	SECURITY CLASSIFICATION AND CODE COUNT UNCLASSIFIED	U025
REPORT NUMBER 1853	1853	CIRCULATION LIMITATION	
REPORT DATE April 1963	0463	CIRCULATION LIMITATION OR BIBLIOGRAPHIC	
		BIBLIOGRAPHIC (Suppl., Vol., etc.)	

SUBJECT ANALYSIS OF REPORT

DESCRIPTOR	CODE	DESCRIPTOR	CODE	DESCRIPTOR	CODE
Rotating	ROTA	Equations	EQUA		
Flow	FLOW	Prandtl (Name)	PRAN		
Flat	FLAT	Motion	MOTI		
Surfaces	SURA	Viscosity	VISC		
Vortex	VORT	Fluids	FLUI		
von Karman (Name)	VONK	Plates	PLAT		
Bodewadt	BOED	Nonlinear	NONI		
Reynolds numbers	REYN	Properties	PROP		
Boundary layer	BOUL	Parameters	PARA		
Theory	THEY	Mathematics	MATH		
Navier-Stokes (Name)	NAVE	Reactors	REAC		
Volterra	VOLS				
Integral (Mathematics)	INTE				
Differential	DIFE				

Naval Weapons Laboratory, Dahlgren, Virginia. (NWL Report No. 1853)
ROTATING FLOWS NORMAL TO A FLAT SURFACE, by E. W. Schwiderski and H. J. Lugt.
Apr 1963. 23 p., 13 figs., 13 tables.
UNCLASSIFIED

Numerical results of three-parameter vortex flows over flat surfaces and of rotating flows of von Karman's and Bodewadt's types are presented for a variety of Reynolds numbers. The new solutions are in good agreement with physical observations. The critical Reynolds number below which Bodewadt flows are laminar, attached, and non-oscillating is computed.

1. Boundary layer - Theory
2. Meteorology
3. Vortex reactor
4. Partial differential equations
I. Schwiderski, E. W.
II. Lugt, H. J.

Task: R360FR103/2101/ R01101001

UNCLASSIFIED

Naval Weapons Laboratory, Dahlgren, Virginia. (NWL Report No. 1853)
ROTATING FLOWS NORMAL TO A FLAT SURFACE, by E. W. Schwiderski and H. J. Lugt.
Apr 1963. 23 p., 13 figs., 13 tables.
UNCLASSIFIED

Numerical results of three-parameter vortex flows over flat surfaces and of rotating flows of von Karman's and Bodewadt's types are presented for a variety of Reynolds numbers. The new solutions are in good agreement with physical observations. The critical Reynolds number below which Bodewadt flows are laminar, attached, and non-oscillating is computed.

1. Boundary layer - Theory
2. Meteorology
3. Vortex reactor
4. Partial differential equations
I. Schwiderski, E. W.
II. Lugt, H. J.

Task: R36FR103/2101/ R01101001

UNCLASSIFIED

Naval Weapons Laboratory, Dahlgren, Virginia. (NWL Report No. 1853)
ROTATING FLOWS NORMAL TO A FLAT SURFACE, by E. W. Schwiderski and H. J. Lugt.
Apr 1963. 23 p., 13 figs., 13 tables.
UNCLASSIFIED

Numerical results of three-parameter vortex flows over flat surfaces and of rotating flows of von Karman's and Bodewadt's types are presented for a variety of Reynolds numbers. The new solutions are in good agreement with physical observations. The critical Reynolds number below which Bodewadt flows are laminar, attached, and non-oscillating is computed.

1. Boundary layer - Theory
2. Meteorology
3. Vortex reactor
4. Partial differential equations
I. Schwiderski, E. W.
II. Lugt, H. J.

Task: R36FR103/2101/ R01101001

UNCLASSIFIED

Naval Weapons Laboratory, Dahlgren, Virginia. (NWL Report No. 1853)
ROTATING FLOWS NORMAL TO A FLAT SURFACE, by E. W. Schwiderski and H. J. Lugt.
Apr 1963. 23 p., 13 figs., 13 tables.
UNCLASSIFIED

Numerical results of three-parameter vortex flows over flat surfaces and of rotating flows of von Karman's and Bodewadt's types are presented for a variety of Reynolds numbers. The new solutions are in good agreement with physical observations. The critical Reynolds number below which Bodewadt flows are laminar, attached, and non-oscillating is computed.

1. Boundary layer - Theory
2. Meteorology
3. Vortex reactor
4. Partial differential equations
I. Schwiderski, E. W.
II. Lugt, H. J.

Task: R36FR103/2101/ R01101001

UNCLASSIFIED